Metal-nonmetal transition in metal-ammonia solutions

Joshua Jortner

Department of Chemistry, Tel-Aviv University, Tel-Aviv, Israel

Morrel H. Cohen

The James Franck Institute and Department of Physics, The University of Chicago, Chicago, Illinois 60637
(Received 25 November 1974)

In this paper we present a coherent physical picture of the metal-nonmetal transition in metal-ammonia solutions in the intermediate concentration range. We propose that in $Li-NH_3$ and $Na-NH_3$ solutions the metallic propagation regime is separated from a nonmetallic regime by a microscopically inhomogeneous regime in which the concentration fluctuates locally about either of two well-defined values M_0 and M_1, $M_0 > M_1$, the local concentration remaining near M_0 or M_1 over radii approximately equal to the Debye short correlation length b for concentration fluctuations. Provided that the concentration-fluctuation decay length is much smaller than b, we can define a percolation problem in which a volume fraction C of the material is occupied by metallic regions of concentration M_0, the remainder containing the low concentration M_1 of dissociated electron-cation complexes. M_0 and M_1 constitute the upper and the lower bounds of the inhomogeneous regime, respectively, while C exhibits a linear dependence on M. This physical picture is borne out by concentration-fluctuation determinations based on chemical-potential measurements in Li and Na solutions and by small-angle x-ray and neutron scattering in Li solutions. Assuming that the phase-coherence length of the conduction electrons is shorter than b and having demonstrated that tunneling corrections are negligible, we can define local electronic structure and transport properties. The limits of the inhomogeneous regime were determined from a combination of concentration-fluctuation measurements, electrical conductivity, Hall effect, and paramagnetic susceptibility data to be $M_0 = 9$ mole percent metal (MPM) and $M_1 = 2(1/3)$ MPM, which yield the C scale, $C = [M - 2(1/3)]/6(2/3)$, for both $Li-NH_3$ at 223°K and for $Na-NH_3$ at 240°K. We have also established the consistency of our picture with the available magnetic data for Na solutions. An analysis of the electronic and the thermal transport properties was carried out in terms of an effective-medium theory, modified to account for scattering from the boundaries of the metallic clusters. For low values of the conductivity ratio ($\sim 10^{-3}$) between the nonmetallic and the metallic regions the modified effective medium theory is valid for $C > 0.4$. In an attempt to mimic the features of continuous percolation, we have carried out numerical simulations of the conductivity in a simple cubic lattice incorporating correlation between metallic bonds. An excellent fit of the experimental conductivity data for Li and Na with the results of the numerical simulations has been obtained over a three order of magnitude variation of the conductivity throughout the entire inhomogeneous regime. A small systematic negative deviation of the conductivity from the predictions of the effective-medium theory for $C > 0.4$ can be properly accounted for in terms of boundary scattering corrections resulting in $b \simeq 15$ Å for Li at 223°K and $b \simeq 32$ Å for Na at 240°K. The overall agreement of the experimental Hall effect, Hall mobility, thermal-conductivity, and thermoelectric-power data with the effective-medium theory is good. The proposed inhomogeneous regime in Li and Na solutions resembles a macroscopic mixed phase at a concentration inside a coexistence curve but with mixing on a microscopic scale. The concentration fluctuations in the inhomogeneous state have nothing to do with critical fluctuations; nevertheless, this state seems to be closely associated with the occurrence of a phase separation.

I. INTRODUCTION

The wealth of information available on metal-ammonia solutions[1-5] (MAS) has resulted in a fairly complete understanding of the physical properties of this system in the extreme concentration limits. Most dilute solutions[6] ($10^{-4}-10^{-3}$ MPM) exhibit the features of electrolytes containing localized solvated electrons[7] and solvated cations. Ionic association involving the formation of solvated electron-cation pairs, and subsequent spin pairing occurs in dilute ($10^{-3}-5 \times 10^{-1}$ MPM) solutions without gross modifications of the structure of the solvated electron.[8,9] Concentrated solutions[10] (10 MPM to saturation) consist of solvated cations, unbound ammonia molecules, and overlapping solvated electrons,[11] constituting a homogeneous amorphous system whose local structure resembles that of a molten salt.[4] Extended electronic states within such an arrangement of electron centers can be described either in terms of the tight-binding approximation or the nearly-free-electron approximation depending on concentration. Near 10 MPM, the separation of the electron centers somewhat exceeds the cavity radius so that the tight-binding approximation is appropriate. On the other hand, near saturation the electron cavities overlap neighboring cavities over most of their surface, so that the nearly-free-electron approximation is appropriate.

The pioneering studies of the electrical conductivity of MAS performed by Kraus about 50 years ago[12] have established the occurrence of a metal-nonmetal transition induced by concentration changes in this two-component system in the intermediate concentration range (1–10 MPM). There MAS exhibit a rapid variation with concentration of many of their static and transport properties.[1-5,13] The following noteworthy phenomena in this transition region are specifically related to the electronic structure and electron transport.
(a) The electrical conductivity[12-15] σ decreases by almost four orders of magnitude (Fig. 1). (b) The Hall coefficient[4,16-19] R increases by a factor of ~6 in the range 10–2.5 MPM (Fig. 1). R exhibits positive deviations from the free-electron value R_{fe} with $R/R_{fe} = 1$ at 10 MPM, $R/R_{fe} = 1.2$ at 5 MPM, and rising to $R/R_{fe} = 2.0$ at 3 MPM. (c) The Hall mobility ($\mu = R\sigma$) exhibits a decrease by two orders of magnitude (Fig. 1) in the range 10–2 MPM. (d) The Knight shifts[4,20,21] at the metal-ion nucleus, K^M, and on the nitrogen nucleus, K^N, decrease with decreasing concentration in the range 10–1 MPM (Fig. 2) and become concentration independent at lower (1–10^{-2} MPM) concentrations.
(e) The paramagnetic susceptibility[13,21] exhibits a minimum around 1 MPM and increases with concentration in the range 1–10 MPM. In Fig. 2 we reproduce the best available data, recently obtained by Lelieur,[21] for the atomic susceptibility χ_p^{at} and for the paramagnetic susceptibility χ_p per unit volume of Na-NH$_3$ solutions. From these experimental results we conclude that χ_p exhibits a linear concentration dependence within the intermediate region (for $M > 3$ MPM). (f) The thermal conductivity[22] exhibits a gradual increase (by a factor of ~3) in the concentration range 1–9 MPM. The thermoelectric power[23] S is negative, revealing a slow increase with decreasing M in the range 9–5 MPM, followed by a break between
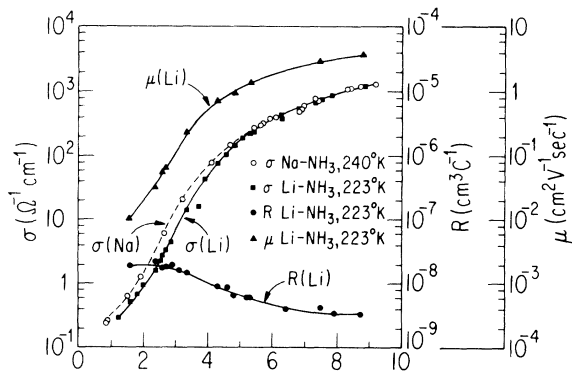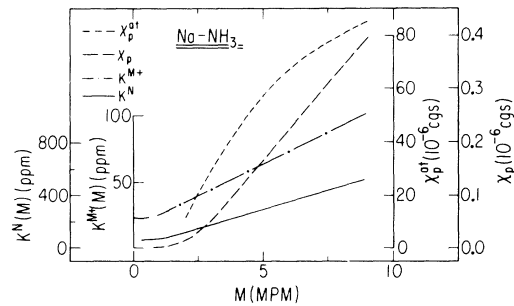

FIG. 2. Concentration dependence of the magnetic data for Na-NH$_3$ solutions at 240 °K (Refs. 4, 13, and 20–22). K^M—Knight shift on the Na$^+$ nucleus; K^N—Knight shift on the N nucleus; χ_p^{at}—atomic paramagnetic susceptibility; χ_p—paramagnetic susceptibility per unit volume.

5–4 MPM, and showing a fast increase below 4 MPM.

In this paper we are concerned with developing a coherent picture of the metal-nonmetal transition in MAS. Before exposing our ideas we shall briefly review the current theoretical background relevant to this problem.

Recent theoretical work on the electronic states and electron transport in one-component systems, such as expanded liquid metals and supercritical metallic vapors, has considered two metallic regimes of electronic conduction which may exist in a disordered system. The propagation, or weak-scattering, regime[24,25] is described in terms of a well-behaved convergent perturbation expansion in powers of the potential. The mean free path l exceeds the reciprocal Fermi wave number k_F^{-1}, i.e., $k_F l \gg 1$, and the transport properties are properly accounted for by the weak-scattering theory and by low-order corrections to the Born approximation. The conductivity is weakly dependent on the density of states at the Fermi energy E_F, R is close to R_{fe}, and μ is dominated by variations in the electrical conductivity. In concentrated MAS (20–10 MPM), Lepoutre[13] and Thompson[26] find that $l = 70$ Å and $k_F = 0.49$ Å^{-1} at 20 MPM decreasing to $l = 12$ Å and $k_F = 0.40$ Å^{-1} at 10 MPM, so that the basic condition for the propagation of conducting electrons between scattering events, $k_F l > 1$, is satisfied down to about 10 MPM. Thus for concentrated (10–20 MPM) MAS solutions, the propagation regime applies. The concentration dependence of σ in the propagation regime was quantitatively accounted for by Russakoff and Aschroft[27a] and by Schroeder and Thompson[27b] in terms of Ziman's weak-scattering model,[28] where the electron scattering centers involve solvated cations and unbound ammonia molecules. The decrease of σ with dilution in the propagation regime is primarily a consequence of the concen-

FIG. 1. Electronic transport data for Li-NH$_3$ and Na-NH$_3$ solutions in the intermediate concentration range taken from Refs. 12 and 15–17.

tration dependence of the structure factors and the increase of the fraction of unbound ammonia molecules.[27] The Hall coefficient[14-16] is $R = R_{fe}$, and the variation of μ is dominated by the changes in σ as expected for the propagation regime.

The second metallic conductivity regime[29-33] involves diffusion, a Brownian type of motion of the conduction electrons. When the phase coherence length of the conducting electrons is comparable to, or less than the spacing between scattering centers, the electrons undergo strong scattering and diffusive motion.[29-31] Friedman has shown[31] that for electron transport in a crystal with a tight-binding s band where the wave-function amplitudes are everywhere constant but the phases are random on different sites, the transport properties are related in the following way:

$$\sigma = \tfrac{2}{3}\pi(e^2/\hbar a)ZX^2 , \qquad (1.1a)$$

$$R = (3\eta \overline{Z}/Z^2)(a^3/ec)X^{-1} , \qquad (1.1b)$$

$$\mu = R\sigma = (2\pi\eta\overline{Z}/Z)(ea^2/\hbar)X , \qquad (1.1c)$$

where Z is the number of nearest neighbors, $\overline{Z}$ is the number of triangular closed paths around each lattice site, $\eta \simeq \tfrac{1}{3}$ is a geometrical factor, a is the intercavity separation, and the parameter

$$X = Ja^3 n(E_F) \qquad (1.2)$$

contains J, the nearest-neighbor electron-transfer integral, and the density of states $n(E_F)$ at the Fermi energy E_F. Since all parameters except X can be readily estimated in particular situations, it is more convenient[32] to relate σ and μ to R_{fe}/R. For the particular case of MAS, we would have

$$\sigma = \left(\frac{6\pi\eta^2}{Z}\right)\left(\frac{\overline{Z}}{Z}\right)^2\left(\frac{e^2}{\hbar a_0}\right)\left(\frac{N}{N_0}\right)^{1/3}\left(\frac{R_{fe}}{R}\right)^2 ,$$

$$\mu = \left(\frac{6\pi\eta^2}{Z}\right)\left(\frac{\overline{Z}}{Z}\right)^2\left(\frac{ea_0^2}{\hbar}\right)\left(\frac{N}{N_0}\right)^{-2/3}\left(\frac{R_{fe}}{R}\right) , \qquad (1.3)$$

where a_0 is the intercavity separation at the electron number density N_0. Friedman[31] has also related in a rough manner the transport coefficients in the diffusion regime to Mott's ratio of the density of states $n(E_F)$ at the Fermi energy to the corresponding free-electron density of states

$$g = n(E_F)/n_{fe}(E_F) \qquad (1.4)$$

and obtained the following approximate relations:

$$R/R_{fe} = Ag^{-1} , \qquad (1.5)$$

with $A = 0.7-1.5$ and

$$\sigma \propto g^2 . \qquad (1.6)$$

From the point of view of general methodology it is important to notice that Friedman's basic hypothesis that the amplitudes of the wave func-

tions are constant is equivalent to the assumption of microscopic homogeneity. Together with Mott[25] we assume[33-35] that Friedman's results are of general applicability for the diffusion regime in a disordered material, provided that the system is microscopically homogeneous with regard to electron transport. From the practical point of view we should like to point out that rough estimates of g, and consequently of $n(E_F)$, can be obtained from transport data via Eqs. (1.5) and (1.6), only if the Friedman relations (1.1) and (1.2) are valid. The signature of the onset of the diffusion regime is the positive deviation of R from R_{fe} [Eq. (1.5)]. For MAS R/R_{fe} exceeds unity for concentrations below 10-8 MPM. One could then argue together with Acrivos and Mott[36,37] that the intermediate-concentration region corresponds to the diffusion regime. However, in the intermediate-concentration regime, relations (1.1) and (1.2) do not hold. Whereas in the concentration range 10-3 MPM R_{fe}/R changes only from 1.0 to 0.5, σ decreases by three orders of magnitude and μ by two orders of magnitude. Acrivos and Mott[36] attempted to derive g from conductivity data. This procedure is unjustified because of the weak concentration dependence of the Hall effect. One could attempt to derive g instead from Knight-shift K or paramagnetic-susceptibility χ_p data, both being proportional to the density of states in a homogeneous metallic regime. For the diffusion regime to hold, the conductivity data must be consistent with[25] $\sigma \propto \chi_p^2$. A $\log_{10}-\log_{10}$ plot of σ vs χ_p displays a slope of 2.3 and not 2, Fig. 3. One might argue that a slope of 2.3 is not so different from one of 2, even though this difference becomes marked over the three-order-of-magnitude variation of σ, but this still leaves the Hall effect unexplained. A similar conclusion follows from analysis of the Knight shift. In subsequent work, Acrivos[37] correlated electrical-conductivity and Hall-effect data according to Eq. (3). Un-
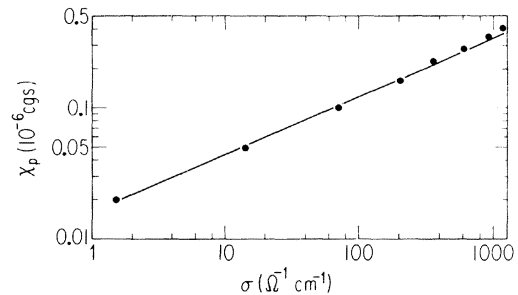

FIG. 3. Conductivity vs paramagnetic susceptibility of Na-NH$_3$ solutions in the intermediate concentration range with the concentration 1—9 MPM being the implicit variable. This $\log_{10}-\log_{10}$ plot results in the empirical relation $\sigma = A\chi_p^{2.3}$.

fortunately, the old Hall-effect data of Kyser and Thompson[16] used by Acrivos[37] were grossly modified in later work by Thompson and his colleagues.[17,18] We conclude that the physical properties of MAS in the intermediate region cannot be accounted for in terms of a diffusion type of metallic transport, and that the metal-nonmetal transition in this system is not preceded by a homogeneous diffusion transport regime as does happen in liquid Hg.[32,34]

On the basis of the foregoing discussion, we assert that the intermediate- (1–10 MPM) concentration region in MAS separates the metallic propagation regime from the electrolyte regime. The metal-nonmetal transition occurs within this intermediate region. There have been several conjectures concerning the nature of the metal-nonmetal transition in this system. Older theoretical work[4,38,39] suggested it to be a Mott transition and used Mott's argument[38] concerning the effects of long-range screening, while subsequent studies focused attention on a Mott transition within a Hubbard band originating from correlation effects.[40] Both approaches would have to be modified to include the effects of randomness of structure in order to account for the general change of the physical properties over the transition region. Recently, Mott and Acrivos[36] have attempted to apply Mott's ideas concerning the formation of a pseudogap,[25,29,41–44] i.e., a range of localized states in MAS when[41,42] $g < g^* \simeq \frac{1}{3}$. The boundaries of the pseudogap are the mobility edges[43,44] and within it the mobility is low. The detailed analysis of Acrivos and Mott[36] did not result in a coherent picture as magnetic and transport properties resulted in different sets of g values.

The role of structural modification and of concentration fluctuations in determining the features of the metal-nonmetal transitions in MAS was considered previously. Cohen and Thompson[4] suggested that while concentrated solutions are characterized by a fused-salt structure, large isolated clusters exist in 1-MPM solutions. The structural aspect of the metal-nonmetal transition was ascribed to the breakup of the fused-salt structure. The idea of clustering in MAS was further pursued by Sienko and Chieux[40] much closer to the critical point. They provided an estimate of the mean cluster size (140 interacting neighbors) from the exponent of the order parameter of the coexistence curve. Lepoutre and Lelieur[13] have proposed that in the intermediate- (1–10 MPM) concentration range MAS are composed of a mixture of metallic aggregates and the bulk dilute solution. On the other hand in an attempt to provide a picture for transport in intermediate MAS, Lelieur, Lepoutre, and Thompson[13b,45] have proposed a spatially homogeneous two-carrier model,

where two types of conduction electrons, characterized by different mobilities, contribute to electronic transport. Such a model[45] is incompatible with the idea of clustering in the intermediate transition region.

We have proposed[35c] that MAS in the intermediate- (1–9 MPM) concentration range are microscopically inhomogeneous,[33,35] with a volume fraction of the material occupied by metallic clusters of a mean concentration of ~ 9 MPM or higher, the remainder consisting of a low concentration (~ 1 MPM) of small, solvated electron-cation complexes. Lelieur[46a] has used that model to account for the temperature and pressure coefficients of the electrical conductivity. Kirkpatrick[47] has also proposed a model of conduction in MAS in this concentration range by percolation through random, inhomogeneously distributed, metallic regions. Here we present an extended and improved version of our model together with applications to a variety of properties of MAS.

We begin by discussing (in Sec. II) the experimental evidence for microscopic inhomogeneities deriving from chemical-potential measurements, x-ray scattering, and neutron scattering. Next, we summarize in Sec. III current theories of electronic structure and transport in such inhomogeneous materials. A prerequisite to applying these theories to MAS is establishing the concentration limits of the inhomogeneous transport regime, which is done in Sec. IV. We then establish the relation between concentration and metallic volume fraction in Sec. V by analysis of the magnetic data; a better lower limit to the inhomogeneous regime also emerges. In Sec. VI we carry out an analysis of the transport data and show that the proposed picture of MAS gives a quantitatively accurate account of the data. Finally in Sec. VII we discuss the implication of our analysis for the thermodynamics and phase diagram of MAS, proposing simple explanations of the phase separation and of the inhomogeneous phase above the consolute point.

II. EVIDENCE FOR INHOMOGENEITIES

Ichikawa and Thompson[48] have found direct evidence for large concentration fluctuations in lithium and sodium ammonia solutions, but not in cesium solutions. They measure the dependence of the chemical potential of the metal on metal concentration and from it extract the mean square concentration fluctuation in the form $\langle (\Delta X_M)^2 \rangle$, where ΔX_M is the fluctuation of the mole fraction. Their results are shown in Figs. 4–6.

Li and Na solutions saturate at 20 and 16 MPM, respectively[4]; the Cs solutions do not saturate.[10] In Figs. 4–6 we compare the observed fluctuations with those expected from an ideal mixture of NH_3
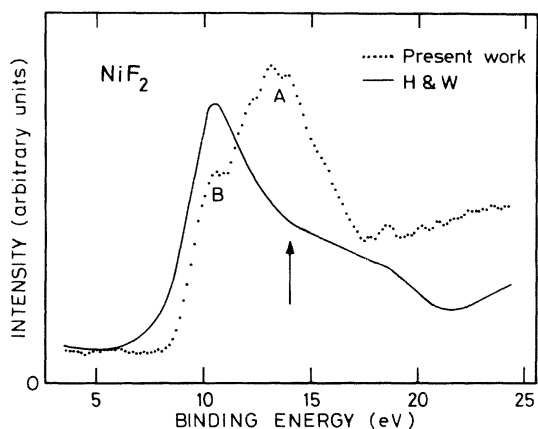
FIG. 4. Mean square of concentration fluctuations in Li-NH$_3$ solutions. Solids lines: experimental data (Ref. 48); dashed line: ideal mixture.

and $M(NH_3)_n$, with $n = 4$ for Li and 6 for Na and Cs:

$$\langle(\Delta X_M)^2\rangle_{ideal} = X_M[1 - (n+1)X_M], \qquad (2.1)$$

where X_M is the mole fraction of metal. The following features of the data are noteworthy: (i) There are large peaks in the Li and Na data centered about 3.6 MPM for Li and a similar value for Na. (ii) These peaks are superimposed on a background similar to what is expected from (2.1). (iii) The background differs from (2.1) in two
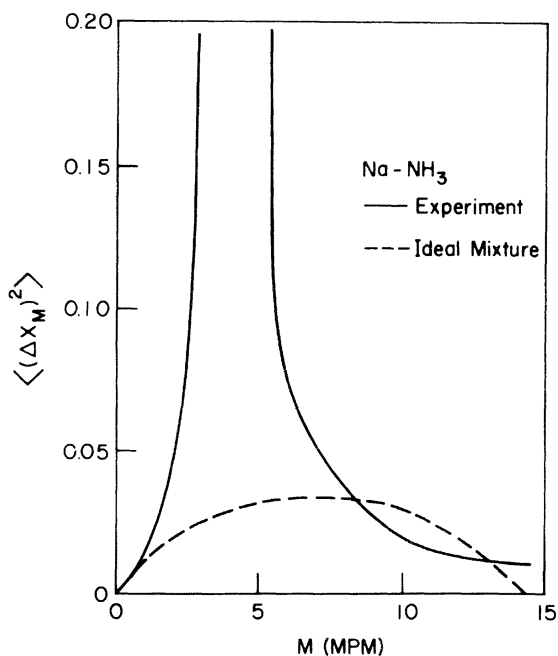

FIG. 5. Mean square of concentration fluctuations in Na-NH$_3$ solutions. Solid line: experimental data (Ref. 48); dashed line: ideal mixture.
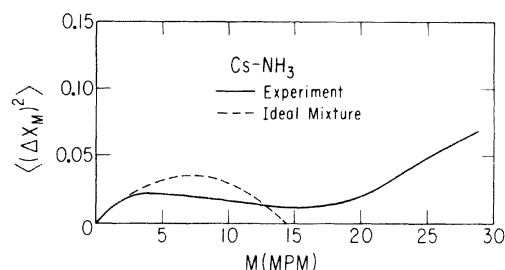

FIG. 6. Mean square of concentration fluctuations in Cs-NH$_3$ solutions. Solid line: experimental data (Ref. 48); dashed line: ideal mixture.

respects, being higher at low concentrations and lower at high concentrations. (iv) Cs shows no peak and its value of $\langle(\Delta X_M)^2\rangle$ is similar to the backgrounds for Li and Na for $M < 16$ MPM. (v) $\langle(\Delta X_M)^2\rangle$ for Cs above 20 MPM resembles what is expected from (2.1) for an ideal mixture of $Cs(NH_3)_6$ and Cs.

Thompson and Lelieur[46b] have pointed out that one can infer by a simple argument of Turner[49] from the excess peaks in $\langle(\Delta X_M)^2\rangle$ for Li and Na the existence of large, high-concentration clusters in those materials. Turner's model was designed for clustering within a homogeneous phase field around a compound composition within that phase field, so that microscopic inhomogeneity vanishes at the compound composition but is present on both sides of it.

In relation to Turner's picture, we propose for Li and Na a picture of the microscopically inhomogeneous region of the phase diagram of MAS in which (i) the concentration fluctuations are bimodal, varying locally about either of two well-defined values M_0 and M_1, $M_0 > M_1$; (ii) the concentration remains near M_0 of M_1 over radii approximately equal to the Debye short correlation length[51] for concentration fluctuations b; and (iii) M_0 is the upper and M_1 the lower bound of the microscopically inhomogeneous region. The concentration fluctuations associated with clusters increase monotonically with cluster size. If the Ornstein-Zernike[50] fluctuation decay length ξ is much smaller than the Debye short correlation length[51] b, the concentration would appear to fluctuate abruptly and randomly from M_0 to M_1 or vice versa. A percolation problem[52-55] is thereby defined in which a continuous region of concentration M_0 is regarded as a metallic cluster. It is a well-known result of percolation theory[55] that the cluster size diverges at volume fraction C of such regions equal to C^*, the percolation probability. However, above C^*, the regions of concentration M_0 which are infinitely extended do not contribute anomalous concentration fluctuations; it is only the bounded clusters which contribute. If ξ is not

much smaller than b, the composition of independent regions of the material of size b into the clusters is not quite a percolation problem because of overlap. For these reasons, one expects a peak in $\langle (\Delta X_M)^2 \rangle$ at the percolation threshold the height of which increases as b increases relative to ξ. We can infer from Figs. 4 and 5 that $M_1 \simeq 2.5$ MPM, $M_0 \simeq 9$ MPM, and $C^* = 0.17$ corresponds to $\simeq 3.6$ MPM for Li. The peak for Na is too strong to make similar assignments, but is not inconsistent with the same values. The value of b/ξ is substantially larger in Na than in Li.

The asymmetry in the background relative to Eq. (2.1) can also be straightforwardly understood for Li and Na. Complexes containing more than one metal atom have formed below 0.1 MPM.[4] These enhance the concentration fluctuations. On the other hand, above 10 MPM the fused-salt structure imposes correlations on an electron cavity and solvated positive ion positions which impede concentration fluctuations.

The over-all behavior of the Cs solutions can be understood as follows. Instead of having saturation at a composition $M(NH_3)_n$, with larger compositions unstable, the "compound" composition and all higher compositions are stable in Cs at high enough temperatures. Small clusters of this compound composition form in a roughly "ideal" solution with NH_3 for $M < 16$ and with pure Cs for $M > 16$ giving a minimum in $\langle (\Delta X_M)^2 \rangle$ at $M = 16$,[46] which corresponds to $n = 6$. In other words, apart from the absence of saturation, the behavior of the Cs solution corresponds to the "background" behavior of the Li and Na solutions. Support for this view of the Cs solutions comes from two sources. First, the nitrogen Knight shift K^N is constant[21c] for concentration above 20 MPM. This can be understood if all of the ammonia molecules are tied up in small clusters of the compound composition $Cs(CH_3)_6$. Second, the liquidus has a sharp temperature minimum[21c] at 16 MPM. This indicates maximum stability of $Cs(NH_3)_6$ in the liquid phase field.

This percolation picture developed for Li and Na solutions is borne out by x-ray[56] and neutron small-angle scattering studies.[57] Schmidt's work[56] on small angle x-ray scattering indicates a Debye short correlation length of 32 Å for Li solutions. It is interesting to note that strong scattering occurs[56] at very small angles at concentrations above our assigned percolation threshold. Recent experiments of Chieux[57] on small-angle neutron scattering on 4-MPM Li-ND$_3$ solutions were analyzed in terms of the Ornstein-Zernike picture of concentration fluctuations. The resulting decay length was $4.7 [T_c/(T - T_c)]^{1/2}$ Å at a temperature T above the consolute temperature T_c, which is $-58\,°C$ for Li-ND$_3$. This decay length is unusually

large, ~ 70 Å at 1 °K above T_c. The study was conducted near the critical concentration, where the bimodal distribution may collapse into a unimodal distribution characteristic of critical fluctuations. It is, however, improbable that critical concentration fluctuations will prevail throughout the whole concentration range 2.3–9 MPM within which the chemical potential data[48] show large fluctuations to exist. Nevertheless, we can use Chieux's results[57] to establish a distance scale for the fluctuations at other concentrations. At 8 °K above T_c, where we analyze the Li-NH$_3$ conductivity data, the Ornstein-Zernike decay length is about 20 Å. We can take this as a rough measure of b elsewhere. Thompson and Lelieur's estimates[46b] of cluster size at 3 and 8 MPM are consistent with a value of b of about 25 Å.

In summary, there is strong experimental evidence favoring microscopic inhomogeneity on a scale of tens of angstroms in NH$_3$ solutions of Li and Na, but not of Cs. We defer attempts to understand the physical origin of the inhomogeneities until after we have explored their consequence for the electronic structure and transport properties of these materials.

III. THEORY OF MICROSCOPICALLY INHOMOGENEOUS MATERIALS

A. Electronic structure

In the preceding section we proposed a picture of Li and Na ammonia solutions in which the local concentration $M(\vec{r})$ in the neighborhood of the point $\vec{r}$ randomly takes on values near 2.5 MPM or near 9 MPM, as the average concentration varies from 2.5 to 9 MPM. Homogeneous solutions of 9 MPM or greater are definitely metallic and in the propagation regime. Solutions below 2.5 MPM are definitely nonmetallic, but only become clearly electrolytic at still lower concentrations, as we shall discuss in Sec. IV later. In our picture, these MAS are undergoing a continuous metal-nonmetal transition in the concentration range ~ 2.5–9 MPM. Clearly, gross changes in local electronic structure must be associated with the local concentration fluctuations, changing from metallic to nonmetallic locally. In order to apprehend how such local nonuniformity of composition can affect the electronic structure or properties, we consider first the autocorrelation function $A(R)$ of the local concentration

$$A(R) = \langle M(\vec{r}) M(\vec{r} + \vec{R}) \rangle - \langle M(\vec{r}) \rangle \langle M(\vec{r} + \vec{R}) \rangle . \quad (3.1)$$

We know from the Ornstein-Zernike theory of fluctuations[50] that asymptotically

$$A(R) \sim e^{-(R/\xi)}/R , \quad (3.2)$$

where ξ is the fluctuation decay length. On the

other hand, $M(\vec{r})$ varies significantly only over distances greater than b, the Debye short correlation length, which must be at least of order an interparticle separation a. The basic structural requirements

$$b > a \ , $$

$$b > \xi \tag{3.3}$$

imply[33-35] that the concentration fluctuations are statistically independent when separated by more than twice the correlation radius. Second, provided that the phase coherence length l is shorter than b, i.e.,

$$b > l \ , \tag{3.4}$$

the electronic structure can be treated semiclassically insuring the validity of the concepts of local electronic structure and local response functions.[33-35,58-63] If the electrons were in the diffusion regime for MAS, the condition (3.4) would be met. However, it will turn out that for MAS (3.4) is not satisfied, and a boundary scattering correction[60] must be included in the transport properties as discussed below. Having made that correction, we can then consider the medium as a submacroscopic inhomogeneous random mixture of regions of radius b which can be treated classically as locally uniform. Accordingly, we can define an allowed volume fraction $C(E)$ of the material actually allowed to electrons of energy E. Now, the Weyl theorem[64] implies that as long as the de Broglie wavelength is sufficiently small compared to the dimensions b of the allowed regions, the density of states will be independent of the geometry of the allowed regions and of the boundary conditions and proportional to the allowed volume. Thus we may take as an approximate definition[62,33-35] of $C(E)$

$$n(E) = C(E)n_0(E) \ , \tag{3.5}$$

where $n_0(E)$ is the density of states per unit volume of a metallic region of macroscopic extent and $n(E)$ is the actual density of states of the microscopically inhomogeneous material. Defined in this way $C(E)$ allows properly for penetration into the excluded regions.

We shall consider now the nature of the electronic states in the metallic regions.[58-63,33-35] If $C(E)$ falls below the critical value C^* for classical percolation,[53-55] percolation theory tells us that a continuous extended path through metallic regions does not exist. If we ignore tunneling through the nonmetallic regions, the metallic wave functions are localized at that energy. If this occurs at the Fermi energy, the system is nonmetallic. The condition for a metal-nonmetal transition in the MAS is therefore[33-35]

$$n(E_F)/n_0(E_F) = C^* \ . \tag{3.6}$$

This result is distinct from

$$g = n(E_F)/n_{fe}(E_F) \simeq \tfrac{1}{3} \ , \tag{3.7}$$

as proposed by Mott[25,29,41-43] for a microscopically homogeneous system. The principal difference between (3.6) and (3.7) is that $n_0(E_F)$ need bear no relation whatsoever to the free-electron density of states. C^* is not sufficiently different from $\tfrac{1}{3}$, which was only an estimate by Mott, to be concerned with. As we shall see below, tunneling corrections are unimportant for MAS.

The continuous site-percolation problem has not yet been solved. Existing numerical studies[55] for three-dimensional lattices give values of C^* ranging from $C^* = 0.195$ for fcc to 0.30 for sc. Zallen and Scher[54] suggest that for percolation in a continuous potential $C^* = 0.15$. Skal, Shklovskii, and Efros[65] find $C^* = 0.17$ for a particular random potential; we use that value and have quoted it above.

We are dealing with an inhomogeneous transport regime in a disordered system, $0 < C < 1$, where we have set $C = C(E_F)$. The inhomogeneous regime can be subdivided into two parts: (a) Pseudometallic regime: $1 > C > C^*$. Above the percolation limit the major contribution to transport originates from the continuous extended metallic paths. The transport properties will exhibit a gradual change from those corresponding to the lower limit of the homogeneous propagation regime (~ 9 MPM). (b) Pseudononmetallic regime: $0 < C < C^*$. Below the percolation limit extended states do not exist, the solution contains isolated finite metallic clusters. Over the pseudononmetallic regime, the transport properties will be intermediate between the pseudometallic and the nonmetallic regimes.

We have thus introduced the notion that the intermediate concentration region should be viewed as an inhomogeneous transport regime where concentration fluctuations lead to localization and to percolation. In the pseudometallic regime, inhomogeneity results in a gradual change of the transport properties and, in particular, a continuous decrease of the conductivity. Percolation at the onset of the pseudononmetallic regime where $C = C^*$ can be viewed as specifying the locus of the metal-nonmetal transition on the phase diagram. Localization in such a disordered system is a consequence of inhomogeneity and is amenable to an approximate description with the aid of semiclassical percolation theory.

B. Modified effective-medium theory for electrical transport

Within the semiclassical approximation, the transport problem becomes equivalent to conduc-

tion in a macroscopically inhomogeneous medium.[66-69] Kirkpatrick[53] has revived the effective-medium theory (EMT) of Bruggeman,[66] Odalev-skii,[67] and Landauer[68] to treat this problem. We have recently constructed[70] an effective-medium theory for the full magnetoconductivity tensor. We shall now briefly outline the results of this transport theory of a randomly inhomogeneous conductor containing regions of two finite but widely different values of the conductivity tensor. The conductivity tensors are $\overleftrightarrow{\sigma}_0$ in the metallic region and $\overleftrightarrow{\sigma}_1$ in the nonmetallic region. These assume the form[70]

$$\overleftrightarrow{\sigma}_i = \sigma_i \overleftrightarrow{I} + \overleftrightarrow{\sigma}_{ia}, \quad i = 0, 1, \tag{3.8}$$

where σ_i is the electrical conductivity and is independent of the magnetic field $\overrightarrow{H}$, while $\overleftrightarrow{\sigma}_{ia}$ is antisymmetric and first degree in $\overrightarrow{H}$. All conductivity tensors will be treated as 3×3 matrices. The macroscopic conductivity tensor for the randomly inhomogeneous conductor

$$\overleftrightarrow{\sigma} = \sigma \overleftrightarrow{I} + \overleftrightarrow{\sigma}_a \tag{3.9}$$

is determined by the effective-medium condition, namely

$$\langle (\overleftrightarrow{\sigma}_i - \overleftrightarrow{\sigma}) \circ (\sigma \overleftrightarrow{I} - \tfrac{1}{3}\overleftrightarrow{\sigma} + \tfrac{1}{3}\overleftrightarrow{\sigma}_i)^{-1} \rangle = 0 . \tag{3.10}$$

Equation (3.10) implies that the fluctuations of the field average to zero and gives the correct relation between macroscopic current and fields. In Eq. (3.10), the average is taken over all possible values of the local conductivities $\overleftrightarrow{\sigma}_i$ and σ_i. Equation (3.10) takes the form

$$\langle (\sigma_i - \sigma)/(2\sigma_i + \sigma) \rangle \overleftrightarrow{I} + 3\sigma \langle (\overleftrightarrow{\sigma}_{ia} - \overleftrightarrow{\sigma})/$$
$$(2\sigma + \sigma_i)^2 \rangle = 0 \tag{3.11}$$

after making use of Eq. (3.8) to first order in $\overrightarrow{H}$. When $\overrightarrow{H} = 0$ one obtains the well-known effective-medium equation for the conductivity[68]

$$\langle (\sigma_i - \sigma)/(2\sigma + \sigma_i) \rangle = 0 . \tag{3.12}$$

The antisymmetric part of the conductivity tensor is obtained from Eq. (3.11) as[70]

$$\overleftrightarrow{\sigma}_a = \frac{\langle \overleftrightarrow{\sigma}_{ia}/(\sigma_i + 2\sigma)^2 \rangle}{\langle (\sigma_i + 2\sigma)^{-2} \rangle} . \tag{3.13}$$

The electrical conductivity σ, the Hall coefficient R, and the Hall mobility μ can then be displayed in the convenient forms[33-35,70]

$$\sigma = f(C, x)\sigma_0 , \tag{3.14}$$

$$\mu = g(C, x, y, f)\mu_0 , \tag{3.15}$$

$$R = h(C, x, y, f)R_0 , \tag{3.16}$$

where the auxiliary functions f, g, and h are

$$f(C, x) = a + (a^2 + \tfrac{1}{2}x)^{1/2} ,$$
$$a = \tfrac{1}{2}[(\tfrac{3}{2}C - \tfrac{1}{2})(1 - x) + \tfrac{1}{2}x] , \tag{3.17}$$

$$g(C, x, y, f)$$
$$= f^{-1}\left(1 - \frac{(2f+1)^2(1-C)(1-xy)}{(2f+1)^2(1-C)+(2f+x)^2C}\right) , \tag{3.18}$$

$$h(C, x, y, f) = g(C, x, y, f)/f(C, x) , \tag{3.19}$$

in terms of the conductivity ratio

$$x = \sigma_1/\sigma_0 \tag{3.20}$$

and the ratio of the Hall mobilities

$$y = \mu_1/\mu_0 \tag{3.21}$$

in the two regions.

The above theory of the low-field magnetoconductivity tensor of an inhomogeneous system is applicable in the inhomogeneous transport regime provided that it is preceded by a homogeneous diffusion regime, when the condition (3.4) is automatically met. In the present case the transport within extended metallic clusters corresponds to the propagation case. That raises the distinct possibility that the mean free path is comparable to the sampling length L, which is twice the Debye short correlation length b.[33-35] In that case, scattering of metallic cluster boundaries reduces the conductivity below the value σ_0 at $C = 1$. The reduction of the metallic conductivity below σ_0 is concentration dependent because the mean cluster size decreases with decreasing concentration. We shall account for the consequent dependence of the conductivity of the metallic region on C by a trivial modification of Eggarter's theory for scattering from the boundaries of the allowed regions.[60] The two conductivities are related by[60]

$$\sigma_0(C)/\sigma_0 = \lambda(C)/l , \tag{3.22}$$

where l is the mean free path at $C = 1$, while $\lambda(C)$ is the mean free path in the allowed volume fraction C. The latter quantity is given by Eggarter in the form[60]

$$\lambda(C) = l\lambda_s/(l + \lambda_s) , \tag{3.23}$$

where in our case the mean free path λ_s associated with scattering by prohibited regions at the boundaries of the allowed regions is

$$\lambda_s = \sum_{n=1}^{\infty} 2nb\, C^{n-1}(1 - C) = 2b(1 - C)^{-1} . \tag{3.24}$$

Thus from Eqs. (3.22)–(3.24) we get

$$D(C) = \sigma_0(C)/\sigma_0 = z/(1 - C + z) , \tag{3.25}$$

where

$$z = 2b/l . \tag{3.26}$$

We impose no corresponding correction to σ_1 from scattering from the boundaries of the nonmetallic region because we expect any correlations among the conducting entities there to decay over distances less than $2b$. We should note in passing

that when the metallic region corresponds to the diffusion limit $z \geq 2b/a$, where a is the interatomic spacing, so that $z \gg 1$ and $D(C) \to 1$ for all C.

The classical expression for the conductivity, Eq. (3.14), has now to be modified by accounting for the dependence of $\sigma_0(C)$ on the fraction of allowed volume, so that

$$\sigma = \bar{f} D(C) \sigma_0 , \tag{3.27}$$

where

$$\bar{f} = f(C, x(C)) , \tag{3.28}$$

$$x(C) = \sigma_1 / \sigma_0 D(C) = x/D(C) , \tag{3.29}$$

and now $x(C)$, Eq. (3.29), replaces x in Eq. (3.17). In a similar way, we can modify Eqs. (3.15) and (3.16) for the Hall coefficient and for the Hall mobility. We assume that the Hall mobility in the metallic regions is affected by boundary scattering in the same way as the "metallic" conductivity. This leads to the following relation:

$$\mu_0(C)/\mu_0 = D(C) . \tag{3.30}$$

Replacing σ_0 and μ_0 in Eqs. (3.15)–(3.21) by (3.25) and (3.30) we get

$$\mu = \bar{g} D(C) \mu_0 , \tag{3.31}$$

$$R = \bar{h} R_0 , \tag{3.32}$$

where Eqs. (3.14) and (3.15) are now modified as follows:

$$\bar{g} = g(C, x(C), y(C), \bar{f}) , \tag{3.33}$$

$$\bar{h} = \bar{g}/\bar{f} , \tag{3.34}$$

$$y(C) = (\mu_1/\mu_0) D(C) , \tag{3.35}$$

and $x(C)$ is given by Eq. (3.25).

Equations (3.25)–(3.35) constitute a complete modified effective-medium theory (EMT z) for the material under consideration. The correction for scattering from the boundaries of the metallic regions modifies the transport equations in two ways. First, σ and μ are proportional to $D(C)$ while no such correction enters for R. Second, the conductivity ratio $x(C)$ and the mobility ratio $y(C)$ which enter into $\bar{f}$, $\bar{g}$, and $\bar{h}$, depend on C via $D(C)^{-1}$. The transport coefficients exhibit the correct asymptotic behavior, i.e., $\sigma \to \sigma_0$, $\mu \to \mu_0$, and $R \to R_0$ when $C \to 1$, while $\sigma \to \sigma_1$, $\mu \to \mu_1$, and $R \to R_1$ for $C \to 0$. In the low-C (< 0.2) region the σ values calculated from the EMT and from the EMT z theory are practically identical, while R and μ are still somewhat sensitive to the value of z.

A few comments on some limiting cases are now in order. For the unphysical case of $x = \sigma_1/\sigma_0 = 0$ the conductivity takes the form

$$\sigma = \sigma_0 (\tfrac{3}{2} C - \tfrac{1}{2}) D(C) , \tag{3.36}$$

while μ and R are independent of y. Kirkpatrick[53]

has shown that Eq. (3.36) [without the $D(C)$ correction term] holds in the range $0.4 < C < 1$. We expect that in this limit the expressions for μ and R are valid over the same range of C values. Kirkpatrick's[53] data and subsequent calculations[71] have demonstrated that for moderately high values of x (≥ 0.05) the effective-medium theory for the conductivity is in good agreement with the results of numerical calculations over the whole region of C; we expect that in this case (3.25)–(3.35) are valid for all C.

In the interpretation of transport in MAS we shall be interested in moderately low values of x ($\simeq 10^{-3}$). Numerical calculations performed by us demonstrate that in the range $0.4 < C < 1$, σ, μ, and R are very close (i.e., within 2% at $C = 0.4$) to their $x = 0$ value, the two latter transport properties being then independent of y. Furthermore, detailed calculations indicate a close agreement between the EMT and numerical results for conductivity in a sc random network. We conclude that for low-x values the effective medium theory and its modified version hold for $C > 0.4$. However, the value of x is so low for MAS that the EMT or the EMT z provides no more than a qualitative guidance in the range $0 < C < 0.4$. Accordingly, we now turn to a numerical simulation of σ in this range, using the methods of Kirkpatrick.

C. Numerical simulation of continuous percolation

As noted above, Kirkpatrick[53] carried out a numerical study of the conductivity of a simple-cubic network of resistors in which each nearest-neighbor bond was randomly assigned a resistance r_0 with probability $1 - C$, and r_1 with probability $1 - C$, $x = r_0/r_1$. He found that effective-medium theory was accurate for $1 > C > 0.4$ independent of x but that serious deviations from the effective-medium theory occurred for small x (≤ 0.05 according to further calculations[71]). In the limit of $x = 0$, the flow of current within the network becomes a bond-percolation process for which the percolation threshold is $C^* = 0.247$,[53,55] the conductivity vanishing for $C < C^*$. EMT gives[33,53,66–68] $\sigma/\sigma_0 = \tfrac{3}{2} C - \tfrac{1}{2}$, $C > \tfrac{1}{3}$, and $\sigma = 0$, $C < \tfrac{1}{3}$, so that $C^*_{\mathrm{EMT}} = \tfrac{1}{3}$. Thus EMT overestimates the value of the percolation threshold for $x = 0$ and can in general be expected to give too low a value of σ for $C < 0.4$ and $x \neq 0$.

It is clear from these results of Kirkpatrick that either an improved formal theory has to be developed for $C < 0.4$ and $x < 0.05$ or that numerical simulation has to be carried out. Yonezawa and Hori[72] have given a formal treatment which improves the EMT, and with Webman we have carried out numerical simulations.[71] We describe our results briefly here; further details will be published separately. First, we note that we are

dealing with a continuous site-percolation problem. Any portion of the material can be randomly metallic or nonmetallic. Second, we note that such a continuum percolation problem has been regarded as the limit of either a site or a bond percolation problem[53b,55] on any lattice as the maximum allowed bond length increases relative to the nearest-neighbor separation. Alternatively, one can impose correlations on neighboring bonds such that if a bond is of one type all its neighbors out to a given correlation distance must be of the same type; the limit of bond percolation as the correlation distance increases is then the continuum percolation problem. As the latter process more closely resembles what occurs in MAS, we have done with Webman[71] numerical simulation of current flow through correlated bonds to evaluate σ for small C and x.

In doing so, we have used modifications of Kirkpatrick's original program[53] which improved convergence and added bond correlation. The results are shown in Fig. 7 for $x = 1.2 \times 10^{-3}$. Curve 1 is effective medium theory, curve 2 is Kirkpatrick's calculation for no bond correlation; and curves 3–5 involve increasingly strong correlation among the bonds. The bond correlation used for curve 3 was constructed by assigning random numbers to each bond, then the 6 bond numbers associated with each vertex were averaged and r_0 or r_1 assigned to the bonds according to the resulting values of the bond numbers. For curve 4, random numbers were assigned to each vertex. Then all 6 bonds leading into it were assigned r_0 or r_1 according to

the vertex number. Finally, for curve 5, the process leading to average bond numbers for curve 3 was iterated once more before r_0 or r_1 was assigned. This second averaging causes a spatial propagation of the bond correlation.

Several features of these results should be noted. For low C (< 0.1), the effective-medium theory yields[71]

$$\sigma/\sigma_1 = (1 - 3C)^{-1} . \qquad (3.37)$$

This can be rewritten

$$\sigma/\sigma_1 = (1 - C/C^*)^{-1} , \qquad (3.38)$$

since $C^* = \frac{1}{3}$ in the EMT. If we reinterpret (3.38) by replacing the EMT value of C^* by the actual value[65,71] 0.17, we find that it accurately fits the numerical values of σ of curve 5. In the transition region $0.1 < C < 0.4$, the numerical results show a systematic trend towards higher conductivity with increasing correlation. This can be most readily understood by reference to the $x \to 0$ case, the strict percolation problem. As we approach continuum percolation by increasing the degree of bond correlation, the percolation threshold decreases from $C^* = 0.247$ for the uncorrelated case, to $C^* = 0.17$. We also confirm Kirkpatrick's conclusion[53] that EMT is accurate for $C > 0.4$, but now under more general circumstances.

It is straightforward to carry out an effective medium theory for any tensorial response function, e.g., thermal transport coefficients, optical constants, diffusion coefficients, etc. Such an EMT case can be readily generalized into an accurate numerical calculation of a random continuum property for a diagonal response function by the method we have used for the electrical conductivity. We have not yet found a way to carry out a network simulation for the Hall coefficient of a random continuum, a nondiagonal response function. It is possible that the systematic procedure of Yonezawa and Hori[72] can yield an improvement over EMT for R.

D. Effective-medium theory for thermal transport

As noted above, the EMT can be extended to handle general response functions in disordered materials. An EMT for the thermal conductivity κ, a diagonal response function, was provided by Odelevskii,[67] while Airapetiants[73] attempted an effective-medium theory for the thermoelectric power. The latter treatment can be criticized on the grounds that it does not involve a self-consistent configurational averaging procedure. We have carried out an EMT for a system simultaneously subjected to gradients of temperature and electric potential, obtaining explicit expressions for the thermal transport properties of an inhomogeneous material.[74]
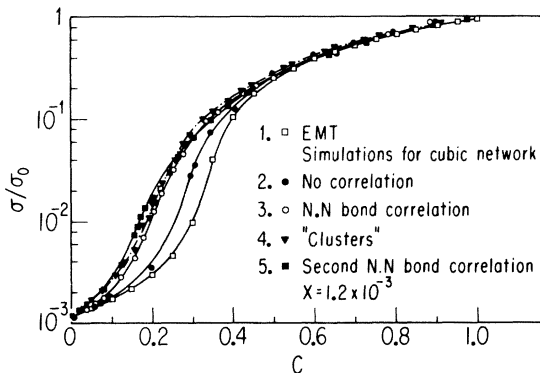

FIG. 7. Numerical results for numerical simulation of continuous percolation. The conductivity of a simple cubic network of conductances with correlated bonds was calculated for a $18 \times 18 \times 18$ network. Values of the conductances are $\sigma_0 = 1$ (with probability C) and $\sigma_1 = 1.2 \times 10^{-3}$ (with probability $1 - C$). Curve 1, □ EMT $x = 1.2 \times 10^{-3}$; curve 2,● Kirkpatrick's model with randomly assigned conductances; curve 3, ○ near-neighbor bond correlation. curve 4, ▼ "metallic clusters" involving nearest neighbors; curve 5, ■ Spatial propagation of bond correlation to second nearest neighbors.

We start with the microscopic equations

$$\vec{J}' = \kappa' \vec{\nabla} T' + P' T' \vec{\nabla} \varphi' \, , \tag{3.39}$$

$$\vec{j}' = \sigma' \vec{\nabla} \varphi' + P' \vec{\nabla} T' \, ,$$

which hold locally within the inhomogeneous material. Primed quantities indicate local values. $\vec{J}'$ and $\vec{j}'$ are the heat and electric currents, respectively, κ' and σ' are thermal and electrical conductivity, respectively. P' is the Peltier coefficient, while φ' and T' are the electrical potential and the temperature, respectively. The corresponding macroscopic equations are identical to (3.39), but with unprimed quantities. The relation between the macroscopic and microscopic fluxes and forces is

$$\vec{J} = \langle \vec{J}' \rangle \, , \quad T = \langle T' \rangle \, , \tag{3.40}$$

$$\vec{j} = \langle \vec{j}' \rangle \, , \quad \varphi = \langle \varphi' \rangle \, ,$$

where the average can be taken equivalently over all space or over all local configurations at a given point.

To carry out an effective medium theory of the relation between the macroscopic transport coefficients κ, σ, and P and the corresponding microscopic quantities, we treat the system as though it consisted of a sphere of radius b embedded within a uniform effective medium characterized by the coefficients κ, σ, and P. We use the conservation conditions and Maxwell's equations together with Eq. (3.39) to determine $\vec{J}'$, $\vec{j}'$, T', and φ' inside the inclusion. Application of Eq. (3.40) results in a consistency condition, the EMT condition, which must be satisfied by κ, σ, and P, determining them implicitly in terms of averages over κ', σ', and P'. The result for σ is the usual EMT result, Eq. (3.12), that for κ was obtained by Odelevskii[67] before

$$\left\langle \frac{\kappa - \kappa'}{\kappa' + 2\kappa} \right\rangle = 0 \, , \tag{3.41}$$

while for P we get[74]

$$P = \frac{3\kappa\sigma \langle P'/(\kappa' + 2\kappa)(\sigma' + 2\sigma) \rangle}{\langle (\kappa\sigma' + \sigma\kappa' + 2\kappa\sigma - \kappa'\sigma')/(\kappa' + 2\kappa)(\sigma' + 2\sigma) \rangle} \, . \tag{3.42}$$

The thermoelectric power S can be obtained from Eq. (3.42) by substituting[75]

$$S = P/\sigma \tag{3.43}$$

for primed and unprimed quantities in (3.42).

The measured thermal conductivity $\bar{\kappa}$ is given by[75]

$$\bar{\kappa} = \kappa - S^2 \sigma T \, . \tag{3.44}$$

For MAS[4,12,13,23] the second term on the right-hand side of Eq. (3.44) is of order $10^{-3} \, \bar{\kappa}$ and can be safely neglected.

The above EMT for thermal transport properties is valid provided that boundary scattering is negligible. Boundary scattering can be introduced as before. The solution of (3.41) for κ in the present case, where κ' takes on the value of κ_0 with probability C and κ_1 with probability $1 - C$, is

$$\kappa = \kappa_0 f(\kappa_1/\kappa_0, \, C) \, , \tag{3.45}$$

with $f(x, C)$ given by Eq. (3.17). As κ' is proportional to the mean free path in the metallic region and insensitive to boundary scattering in the nonmetallic regions, the EMT z for σ can be taken over directly for κ,

$$\kappa = \kappa_0 D(C) f(\kappa_1/\kappa_0 D(C), \, C) \, . \tag{3.46}$$

The operational definition of the Lorentz number is

$$L = \frac{\kappa - \kappa_{\text{nonel.}}}{\sigma T} \, , \tag{3.47}$$

where κ and σ are measured quantities and $\kappa_{\text{nonel.}}$ is an estimated nonelectronic contribution to the thermal conductivity. For a uniform metallic system, L is close to $L_0 = 2.45 \times 10^{-8} \, \text{W} \, \Omega \, \text{K}^{-2}$. In the inhomogeneous regime, there is no longer additivity in the conductivities and L can in principle deviate considerably from L_0. Indeed, there is no clear cut procedure for defining $\kappa_{\text{nonel.}}$.

E. Tunneling corrections

From the analysis of Sec. III C, it is clear that for values of x as low as those pertaining to MAS, percolation effects play a prominent role in determining the concentration variation of the electrical conductivity and other transport properties, especially for values of C below the percolation threshold $C^* = 0.17$. If tunneling across the nonmetallic regions were important,[76] the local nonmetallic conductivity would be shorted out by tunneling, transport would no longer be by percolation, and the quantitative details of the present theory would be wrong. Accordingly, we estimate tunneling corrections in the present subsection.

Below C^*, the metallic regions can be considered isolated clusters of radius b embedded within the nonmetal with average separation $2R_s$. The mean free path in the metallic regions is about 12 Å,[13] and we are just at the borderline between the propagation and diffusion regions. We choose to carry out the tunneling calculation by ignoring phase incoherence; this should yield an upper limit to the tunneling conductance per unit area between two clusters, G. Standard tunneling theory then yields the form

$$G = [\sigma_G/2(R_s - b)]|T|^2 \, , \tag{3.48}$$

where

$$\sigma_G = 3Ne^2 \lambda_d / p_F , \tag{3.49}$$

$$\tfrac{1}{4} \lambda_d = (\hbar^2/2m)^{1/2}(W - E_F)^{3/2}/W^2 \tag{3.50}$$

is of the order the decay length of the wave function inside the barrier, of height W above the bottom of the conduction band, and p_F is the Fermi momentum. Finally, in (3.48) the tunneling probability across the barrier is

$$|T|^2 = \exp\{- 2[2m(W - E_F)/\hbar^2]^{1/2} 2(R_s - b)\} . \tag{3.51}$$

The electronic energy within the metallic clusters is estimated via a simple model of the conduction electron energies [Cohen, Jain, and Jortner (CJJ) (unpublished)]. In that model, the energy of an electron at the bottom of the conduction band is

$$E_M = E_0 - \Delta E_0 - \alpha e^2/D r_{+-} + E_{sc} + E_c .$$

Here $E_0 = - 2$ eV is the lowest energy level of an electron in an isolated cavity [Gaattou and Jortner[3] (GJ)]; $- \Delta E_0$ is the Wigner-Seitz shift of that level imposed by the vanishing of the radial derivative of the corresponding eigenfunction midway between the cavities. The next term is the Madelung energy of a zinc-blende-like arrangement of ions (CJJ) with a Madelung constant α of 1.64, an effective dielectric constant D of 5.5 (CJJ), and a separation between neighboring positive ions and electron cavities r_{+-} of 5.5 Å, yielding $- 0.48$ for the Madelung energy. E_{sc} is the change in the Coulomb interactions between neighboring cavities caused by metallic screening, and E_c is the exchange and that part of the correlation energy not already included in the Madelung energy. CJJ have argued that E_{sc} and E_s are relatively small at 9 MPM, as the electrons are rapidly approaching the tight-binding limit (see Sec. I) with decreasing concentration. For similar reasons, we also neglect ΔE_0. The barrier height W is given by

$$W = V_0 - E_m ,$$

where $V_0 = - 0.25$ eV (GJ) is the bottom of the conduction band in pure NH_3, or $W = 2.23$ eV. A free-electron approximation gives 0.58 eV for E_F so that $W - E_F$ is 1.7 eV or $\simeq 2$ eV. G is to be compared with the conductance associated with the nonmetal

$$G_1 = \sigma_1/2(R_s - b) . \tag{3.52}$$

For tunneling corrections to be negligible, we require that

$$G/G_1 \ll 1 . \tag{3.53}$$

Inserting (3.48), (3.49), and (3.52) into (3.53) gives for that condition

$$(3\lambda_d/lx)|T|^2 \ll 1 , \tag{3.54}$$

where we have used a nearly-free-electron approximation for σ_0,

$$\sigma_0 = Ne^2 l / p_F , \tag{3.55}$$

N being the conduction-electron density. Making use of the relation

$$R_s = bC^{-1/3} , \tag{3.56}$$

and choosing the smallest possible value of b indicated by any of the data presented or still to be presented in this paper for Li or Na, $b = 15$ Å, we obtain an upper limit for $|T|^2$ of 10^{-14} for $C = 0.1$ and of 10^{-11} for $C = 0.15$. The values of W and $W - E_F$ cited above with $l = 12$ Å, give

$$G/G_1 = 10^2 |T|^2 . \tag{3.57}$$

Condition (3.53) is always satisfied, and tunneling corrections are negligible in these systems. We conclude that we can proceed safely to the analysis of the transport properties of MAS via semiclassical transport theory.

IV. LIMITS OF INHOMOGENEOUS REGIME

Fitting the theory to the experimental transport properties of MAS in the inhomogeneous regime requires the following: (a) Identification of the limits of the inhomogeneous transport regime. (b) Determining the values of the transport coefficients at those limits, $C = 0$ and $C = 1$; and (c) establishing the relationship between C and M. We consider (a) and (b) in the present section; (c) is carried out in Sec. V.

Regarding the upper limit, $C = 1$, we have already noted that the anomalously large concentration fluctuations[48] disappear into the background at $M \simeq 7-9$ MPM in the Li and Na solutions, Figs. 4 and 5. It is interesting that the Hall constant[16-19] R for Li begins to exceed the free-electron value R_{fe} for $M < 9$ MPM. Furthermore, the conductivity[12-15] there becomes of order $10^3 \, \Omega^{-1} \text{cm}^{-1}$ for Li and Na solutions and that $k_F l$ approaches[4,13] the value of $k_F l \simeq 3$ at 9 MPM for Li and Na, while in the case of expanded liquid Hg,[32] the propagation regime does not apply only for $k_F l < 2.3$. These three facts together indicated the termination of the homogeneous propagation regime in MAS at 9 MPM. The Hall-effect data for Li together with the conductivity data for Li and Na provide at present the principal reason for choosing $M = 9$ MPM to constitute the lower limit of the homogeneous propagation regime; concentration fluctuation data[48] are consistent with this choice. Below 9 MPM the linear relationship (1.3) between σ and $[N/N(9)]^{1/3} R^{-2}$ required in the diffusion regime fails seriously. Accordingly, in Li and Na solutions the termination of the propagation regime is not associated simply with the onset of the diffusion regime. Coupling these facts about the transport properties with the evidence for inhomogeneity exposed in Sec. II leads us to identify the upper

limit of the inhomogeneous transport regime as C = 1 at 9 MPM in Li and Na solutions.

Turning now to the lower limit, $C = 0$, the concentration fluctuations[47] in Li solutions, Fig. 4, suggest that the material becomes homogeneous again at $M \simeq 2.5$ MPM. On the other hand, an electrolyte model is inconsistent with the transport data[12-15] down to 1 MPM for Li and Na. At 1 MPM the equivalent conductance has already reached a value as large as can possibly be expected from the electrolyte picture. It increases further by an order of magnitude in the range 1-2.5 MPM, a change which cannot be encompassed within an electrolyte model. We therefore have previously considered[47] 1 MPM as the onset of the inhomogeneous transport regime. That would correspond to a value of x of 2×10^{-4}, and the conductivity would be given by (3.38) for small C. Equation (3.38) implies an increase in σ by 2.5 for $C = 0.1$ over its value σ_1, at $C = 0$. That in turn implies that $C = 0.1$ at 1.7 MPM. That such a value for M for $C = 0.1$ cannot be reconciled with both the magnetic data and the conductivity at high concentrations is implicit in the later sections of this paper. Accordingly, we set $M \simeq 2.5$ MPM as the lowest limit, $C = 0$, of the inhomogeneous regime, and refine this value of M for $C = 0$ to 2.3 MPM by analysis of the magnetic data in Sec. V.

We note in passing that this assignment of the lower limit of the inhomogeneous regime at $M = 2.3$ MPM requires a reinterpretation of the transport properties of MAS in the concentration range 1-2.3 MPM. At 1 MPM the equivalent conductance is[4] 770 cm^2 Ω^{-1} mole^{-1}, equal in value to the limiting equivalent conductance which is the upper limit of the conductivity in the electrolytic transport regime. We recall that the paramagnetic susceptibility of Na-NH$_3$ solutions[21] is close to zero at 1 MPM, whereupon complete spin pairing occurs. In the concentration range 1-2.3 MPM the paramagnetic susceptibility[21] increases to 0.08×10^{-6}

cgs while the conductivity[12-16] rises from 0.15 to 1 $(\Omega \, \text{cm})^{-1}$, the low value of σ implying nonmetallic electronic transport in that concentration region. We suggest that pseudointrinsic semiconducting transport[25,34] is operative in MAS in the concentration region 1-2.3 MPM. The full valence band and the empty conduction band correspond to superposition of σ_g- and of σ_u-type orbitals of (doubly occupied) electron cavity pairs, respectively. The $\sigma_g - \sigma_u$ splitting of a single cavity pair at low concentrations is 0.6-0.7 eV. Thermal excitation occurs across the mobility gap. This transport mechanism in MAS is analogous to that exhibited in expanded liquid Hg in the semiconducting transport regime[34] at densities below 7.8 g cm^{-3}.

The corresponding values of the parameters needed as input data for the transport properties are taken from experiment[12,14-17,22,23] and listed in Table I for Li and Na solutions. They yield

$$x = 1.2 \times 10^{-3}, \quad \text{Li-NH}_3 \ 223 \ ^\circ\text{K},$$
$$x = 2.4 \times 10^{-3}, \quad \text{Na-NH}_3 \ 240 \ ^\circ\text{K}, \tag{4.1a}$$
$$y = 7.9 \times 10^{-3}, \quad \text{Li-NH}_3 \ 223 \ ^\circ\text{K}, \tag{4.1b}$$
$$\kappa_1/\kappa_0 = 0.35, \quad \text{Na-NH}_3 \ 240 \ ^\circ\text{K}, \tag{4.1c}$$
$$S_1/S_0 = 20, \quad \text{Na-NH}_3 \ 240 \ ^\circ\text{K}. \tag{4.1d}$$

Before we can use these parameters in the analysis of the transport data, we require C vs M, a C scale, also obtained in Sec. V.

V. ANALYSIS OF MAGNETIC DATA AND C SCALE

The best available data for the spin susceptibility[21] are shown in Fig. 8. For Na solutions χ_p becomes appreciable above 1 MPM, increasing monotonically with M. It is linear with M in the range $3 < M < 9$ MPM, where it follows

$$\chi_p = \tfrac{1}{7}(M - 2)\chi_m, \tag{5.1}$$

where $\chi_m = \chi_p(9)$ is the volume susceptibility in the

TABLE I. Values of electronic and thermal transport coefficients associated with the inhomogeneous transport region in Li and Na MAS.

C	M (MPM)	σ $(\Omega \, \text{cm})^{-1}$ Li-NH$_3$ 223 °K	Na-NH$_3$ 240 °K	R (cm^3/C) Li-NH$_3$ 223 °K	μ (cm^2 V^{-1} sec^{-1}) Li-NH$_3$ 223 °K	S (μV K^{-1}) Na-NH$_3$ 240 °K	Li-NH$_3$ 230 °K	κ (W cm^{-1} K^{-1}) Na-NH$_3$ 240 °K	Remarks
0	2.33	1.5	3.0	1.9×10^{-3}	0.031		−49.5	3.8×10^{-3}	Lower limit
0.17	3.47	18	33	1.3×10^{-3}	0.26	−17	−33	3.9×10^{-3}	Percolation threshold
0.4	5.00	180	190	6.6×10^{-4}	1.15	−7.6	−4.1		Onset of validity of EMT for σ
2.0	9.0	1210	1240	3.1×10^{-4}	3.9	−2.8		9.4×10^{-3}	Upper limit

metallic regions. Below 3 MPM, the data are in-
sufficient to establish uniquely a dependence such
as (5.1). They can be fitted either to a continua-
tion of (5.1) to 2.3 MPM plus another linear seg-
ment from 2.3 to 1 MPM or to (5.1) to 3 MPM
plus a quadratic segment from 3 to 1 MPM. It
should be noted that the relation (5.1) continues[21]
above $M = 9$ MPM, so that the magnetic data are
useless for establishing an upper limit to the in-
homogeneous regime. Instead, we shall use them
to establish a lower limit and a dependence of C
upon M within the inhomogeneous regime.

The model we use to interpret χ_p is the same
we have used for the concentration fluctuations and
the transport properties. The material consists
of a random mixture of metallic regions of mean
concentration 9 MPM and nonmetallic regions of
mean concentration M_1 which is to be determined.
The metallic regions have volume susceptibility
χ_m, and the nonmetallic χ_1. Because local field
corrections are negligible in χ_p, effective medium
theory is unnecessary, and we can write[77]

$$M = 9C + (1 - C)M_1 ,\qquad (5.2)$$

$$\chi_p = C\chi_m + (1 - C)\chi_1 .\qquad (5.3)$$

Inserting (5.1) for χ_p in (5.3), and defining

$$r = \chi_1 / \chi_m ,\qquad (5.4)$$

gives us

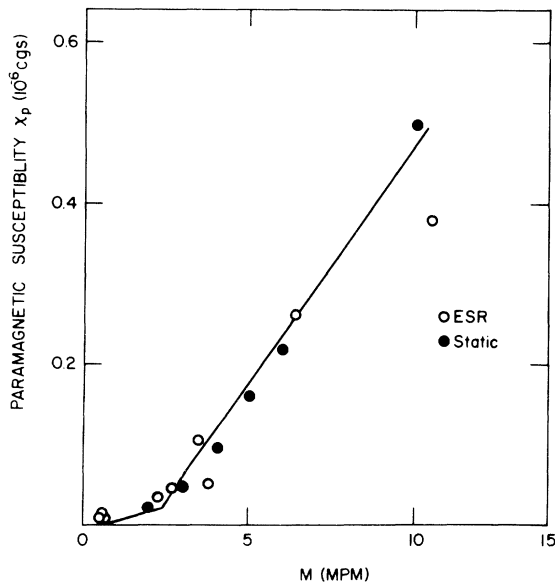$$C = (M - M_1)/(9 - M_1)\qquad (5.5)$$

for the C scale, and the relation

FIG. 8. Fit of the two-linear-segment function Eqs.
(5.1) and (5.7), to the experimental paramagnetic sus-
ceptibility data (Ref. 21) for Na-NH$_3$.

$$M_1 = 2 + 7r\qquad (5.6)$$

between the two parameters M_1 and r.

Since χ_p is linear in M at least down to 3 MPM
and C is linear in M according to (5.5), (5.3),
plus (5.6) imply that $2 < M_1 < 3$ MPM. Accordingly
we have to introduce a fitting function for χ_p in
that range. We have considered two possibilities:
(i) two linear segments, Eq. (5.1) for $M > 2\frac{1}{3}$ MPM
and

$$\chi_p = \frac{1}{28}(M - 1)\chi_m\qquad (5.7)$$

for $M < 2\frac{1}{3}$ MPM; (ii) a linear segment, Eq. (5.1)
for $M > 3$ MPM and a quadratic segment

$$\chi_p = \frac{1}{28}(M - 1)^2 \chi_m\qquad (5.8)$$

for $M < 3$ MPM. Inserting M_1 into (5.7) and (5.8)
to give χ_1 and r gives $M_1 = 2\frac{1}{3}$ and 3 MPM, respec-
tively, upon insertion of the resulting r values into
(5.6). That the value 3 MPM is well within the
inhomogeneous regime is indicated by the concen-
tration fluctuation data,[46] which show anomalies
already at 2.5 MPM in Li. The peak fluctuation
occurs at about 3.7 MPM while the values of M at
which $C = C^*$ are 3.5 and 4.0 MPM for the linear
and quadratic fits, respectively, favoring $M_1 = 2\frac{1}{3}$
slightly. However, the most important basis for
selecting $M_1 = 2\frac{1}{3}$ as the lower limit to the inhomo-
geneous regime is that the fit to the conductivity
data is worse for $M_1 = 3$ MPM. Accordingly, we
choose our C scale as

$$C = (M - 2\frac{1}{3})/6\frac{2}{3}\qquad (5.9)$$

and show in Fig. 8 the corresponding fit of the two
linear segment function to the χ_p data.

We now turn to the correlation between Knight
shift[4,20,21] and volume susceptibility. We are deal-
ing with the limit of extreme motional narrowing for
the nuclear resonance. As a consequence, the
observed Knight shift is the mean of the Knight
shift in the metallic regions K_m, and that in the
nonmetallic regions K_1 weighted by the proportion
each region contributes to the nuclear volume sus-
ceptibility χ_T^n

$$K = K_m(\chi_m^n / \chi_T^n)C + K_1(\chi_1^n / \chi_T^n)(1 - C) ,\qquad (5.10)$$

where χ_m^n and χ_1^n are the nuclear volume susceptibi-
lities in the metallic and nonmetallic regions, re-
spectively. As each nuclear susceptibility is
proportional to the corresponding nuclear number
density, (5.10) can be rewritten[78]

$$\bar{N}K = K_m N_m C + K_1 N_1(1 - C) ,\qquad (5.11)$$

where $\bar{N}$ is the mean metal atom number density,
N_m is that quantity in the metallic regions, and N_1
the same in the nonmetallic regions. Comparing
(5.11) with the corresponding relation for the
volume susceptibility χ_p, we see that our model
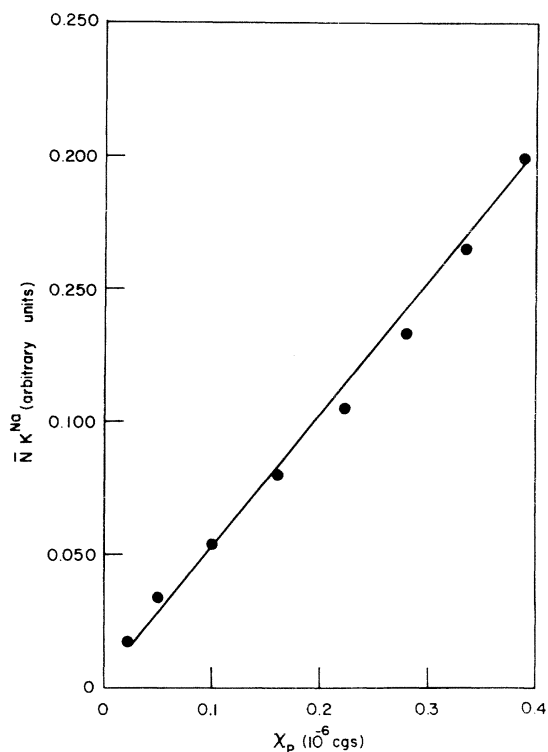
FIG. 9. Paramagnetic susceptibility vs $\bar{N}K$ of Na-NH$_3$ solutions (Refs. 20–22) with the concentration (2–9 MPM) being an implicit variable.

predicts a linear relation between $\bar{N}K$ and χ_p. A plot of $\bar{N}K$ and χ_p is displayed in Fig. 9, and a linear relation is found to hold over the inhomogeneous regime and, indeed, outside of it. This correlation between $\bar{N}K$ and χ_p can evidently not be used to fix the limits of the inhomogeneous regime since a similar relation is expected to hold in the homogeneous metallic regime in any event.

The increase in χ_p above its minimum value actually starts at 1 MPM, and the equivalent conductance there increases above the maximum that could be expected from an electrolyte. Both facts support an electronic contribution to the conductivi-

TABLE II. Inconsistency of magnetic and conductivity data in the concentration range 1–2.3 MPM with the inhomogeneous transport regime.

M MPM	$\sigma(M)/\sigma(9)$	(from σ)[a]	(from χ_R)[b]
1	1.8×10^{-4}		
1.24	2.5×10^{-4}	0.046	0.009
1.6	4.3×10^{-4}	0.097	0.025
2.0	7.8×10^{-4}	0.128	0.038

[a]Calculated from $C = \frac{1}{6} [1 - \sigma(1)/\sigma(M)]$.

[b]Calculated from $C = \chi_p/\chi_m$ or, alternatively, estimated from $C = \frac{1}{28} (M - 1)$.

ty, and raise the possibility that the onset of inhomogeneity occurs at $M = 1$ instead of 2.3 MPM as proved Sec. IV. However, it is not possible to make mutually consistent interpretations of the conductivity and paramagnetic susceptibility on that basis. The conductivity for low C is given by Eq. (3.38) with $C^* \simeq 0.17$; values of C derived therefrom are shown in Table II. The spin susceptibility in this region is given by Eq. (5.7) below $M = 2\frac{1}{3}$, using the fit of χ_p to two linear segments. The inhomogeneous model then gives

$$C = \frac{1}{28}(M - 1) , \quad M < 2\frac{1}{3} , \qquad (5.12)$$

which is also shown in Table II. The two sets of value of C differ drastically, confirming our previous conclusion that the inhomogeneous regime starts at $M = 2.3$ MPM.

Having established the consistency of our picture of an inhomogeneous regime in Li and Na ammonia solutions, we can now proceed to an analysis of the transport data using the C scale thereby defined.

VI. ANALYSIS OF TRANSPORT DATA

A. Conductivity

Our numerical simulations show that the EMT holds accurately for $1 > C > 0.5$ or $9 M > M > 5.5$ MPM. Moreover, the EMT reduces to its $x = 0$ form $\sigma/\sigma_0 = \frac{3}{2}C - \frac{1}{2}$ for values of x as small as we are dealing with here (see Table I). Accordingly, we have compared σ/σ_0 with $\frac{3}{2}C - \frac{1}{2}$ for Li and Na for $9 > M > 5.5$ MPM and show the results in Figs. 10 and 11. The data fall systematically below the
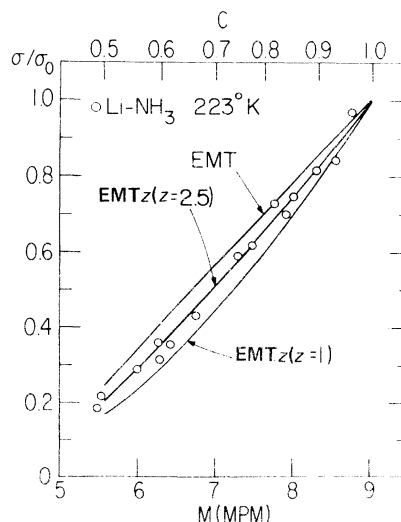

FIG. 10. Analysis of the electrical conductivity data of Li-NH$_3$ solutions, $5.5 < M < 9$ MPM, at $T = 223$ °K (Refs. 14–17) in terms of the modified effective-medium theory (EMT z). The best fit is obtained for $z = 2.5$. The curves for $z = \infty$ (EMT) and for $z = 1$ are shown for comparison.

EMT, more so for Li than for Na. We therefore
fitted the data to the EMTz, Eqs. (3.27)–(3.29)
adjusting the one parameter z to get a best fit.
The results are also shown in Figs. 10 and 11 for
the best fit of $z = 2.5$ for Li while a least-square
analysis results in $z = 5.3 \pm 0.6$ for Na. Also shown
is EMTz for $z = 1$ for comparison.

From these values of z a rough estimate of b
can be obtained. Using the weak scattering, nearly-
free-electron form for σ_0, we estimate the mean
free path to be 12 Å for Li and Na. The corre-
sponding values of b from Eq. (3.26) are

$$b = 15 \text{ Å}, \quad \text{Li–NH}_3, \quad T = 223 \text{ °K},$$
$$b = 32 \text{ Å}, \quad \text{Na–NH}_3, \quad T = 240 \text{ °K}. \quad (6.1)$$

These results are quite remarkable in that rough,
quantitative, microscopic structural information
has been obtained from the electrical conductivity.
The numerical value of 15 Å for Li is consistent
with the x-ray and neutron scattering data[56,57] con-
sidering the uncertainty attached to the estimate
of the mean free path, etc. Moreover, the am-
plitude of the fluctuation peak scales with the cube
of b so that the factor of 2.1 increase in b in going
from Li to Na is enough to account for the striking
increase in the peak height for concentration
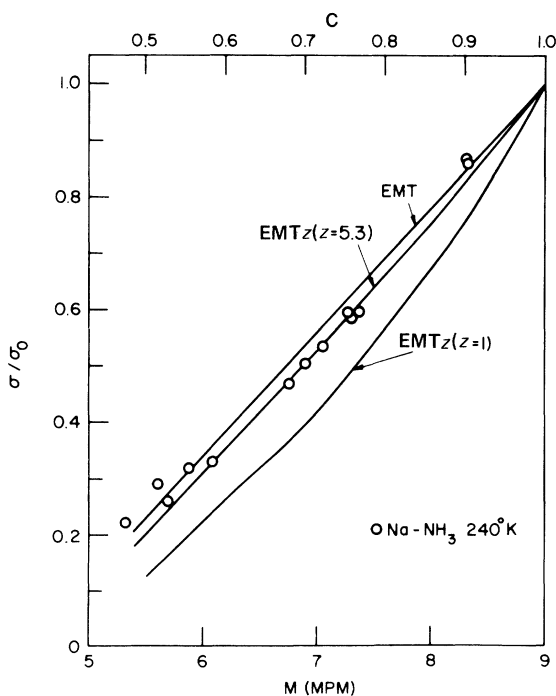fluctuations in Na over Li, as is evident from
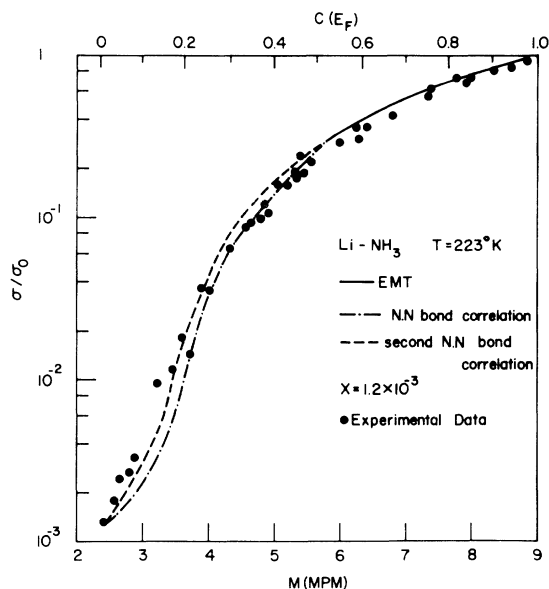Figs. 4 and 5.

FIG. 12. Analysis of the electrical conductivity data
of Li–NH$_3$ solutions at 223 °K (Refs. 12–15 throughout
the entire inhomogeneous regime. $C = 1$ at 9 MPM and
$C = 0$ at 2.33 MPM. Solid Curve ($C > 0.5$): EMT; dotted-
dashed curve: numerical simulation with nearest-neigh-
bor bond correlation ($x = 1.2 \times 10^{-3}$); dashed curve: nu-
merical simulation with second nearest-neighbor bond
correlation ($x = 1.2 \times 10^{-3}$); circles represent experimental
data.

FIG. 11. Analysis of the electrical conductivity data
of Na–NH$_3$, $5.5 < M < 9$ MPM, at $T = 249$ °K (Ref. 12) in
terms of the EMT z. The best fit is obtained for $z = 5.3$
± 0.6. Also shown are the curves for $z = \infty$ and $z = 1$.

The fit to the EMT breaks down seriously at low
concentration and the EMTz is little different there.
Accordingly, we have compared the experimental
data with various numerical simulations in Figs.
12 and 13 for Li and for Na. One sees that as the
correlation is increased so that continuum percola-
tion is approached, the fit becomes excellent over
3 orders of magnitude of variation in σ. It should
be recognized that the theoretical curve is fixed
to the experimental data at the $C = 0$ and $C = 1$ end
points of the inhomogeneous range but that other-
wise there are no adjustable parameters. (We
have ignored the EMTz corrections in the present
context.) The simulations should be regarded,
therefore, as interpolations between the end points
and they serve excellently as such. There should
be little doubt now as to the existence of an in-
homogeneous transport regime for $2.3 M < M < 9$
MPM.

On the basis of the preceding analysis we criti-
cize Lelieur's calculations[46] of the temperature and
pressure coefficients of σ on two points: (i) the
use of the limits 1–9 MPM for the inhomogeneous
regime instead of 2.3–9 MPM and (ii) the use of
the EMT in the low-C range, $C < 0.4$, the region
of interest for the temperature and pressure coef-
ficients. We note in passing that the maximum in
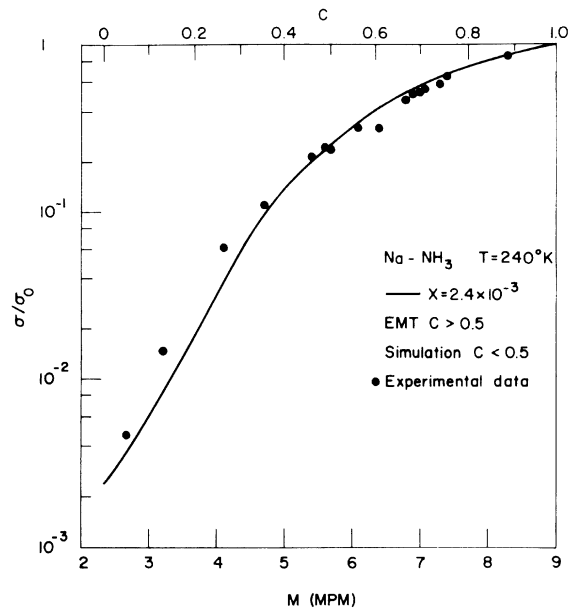the temperature coefficient of σ (2.0 MPM for Na–

FIG. 13. Analysis of the electrical conductivity data of Na-NH₃ solutions at 240 °K (Ref. 12) throughout the entire inhomogeneous regime. $C = 1$ at 9 MPM and $C = 0$ at 2.33 MPM. Solid curve: EMT for $C > 0.5$ and numerical simulations with second nearest-neighbor bond correlation ($x = 2.4 \times 10^{-3}$) for $C < 0.5$; circles represent experimental results.

NH₃ and 2.8 MPM for Li-NH₃ solutions) occurs close to $C = 0$, while the minimum in the pressure coefficient (3.5 MPM for Na-NH₃ solutions) is exhibited near $C = C^*$. In the absence of adequate information on the temperature and pressure dependence of the C scale we defer further analysis of this problem.
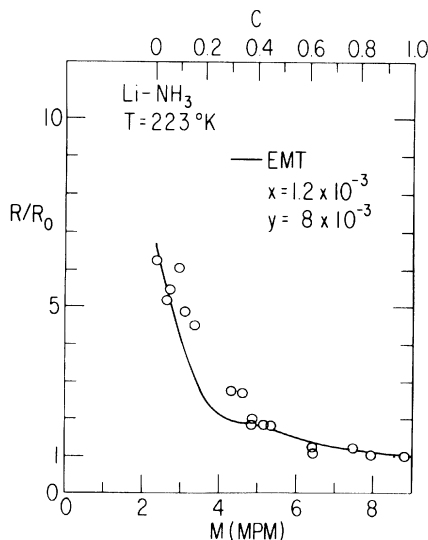

FIG. 14. Analysis of Hall-effect data (Refs. 18 and 19) of Li-HN₃ solutions at 223 °K in terms of the EMT.
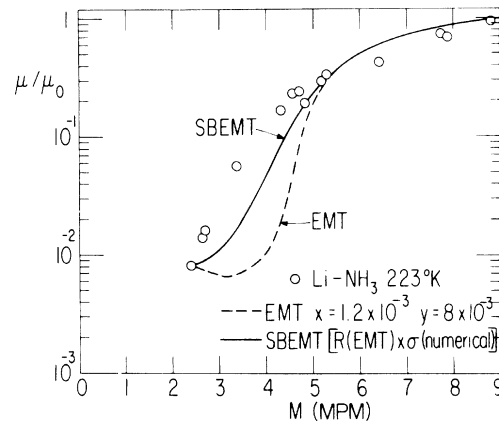

FIG. 15. Analysis of the Hall-mobility data (Refs. 16 and 17) for Li-NH₃ solution at 223 °K in terms of the effective-medium theory (dashed line) and the SBEMT (solid line).

B. Hall data

Since we have been unable to go beyond the EMT for the galvanomagnetic properties, we have compared the available Li Hall data[16–19] to the effective-medium theory. As we have noted in Sec. III the boundary scattering corrections to R are negligible for $C > 0.4$, while in the low-C range ($0 < C < 0.4$) the EMT is inaccurate, and there is little point to introduce the modified EMT z version of the theory. In Fig. 14 we portray the available Li Hall effect data together with the EMT curve using the experimental data at $C = 0$ and $C = 1$ from Table I. In the pseudometallic regime down to $C = 0.4$ the agreement between theory and experiment is good, while for $0 < C < 0.4$ the EMT curve provides just an approximate interpolation formula.

In view of the quantitative agreement of σ and R with the predictions of the EMT (and EMT z) in the range $0.4 < C < 1$ it is apparent that a good fit can be obtained for the concentration dependence of the Hall mobility μ in this range as is evident from Fig. 15. The small negative deviations of μ from the EMT curve in the concentration range $5 M < M < 9$ MPM can be readily accounted for in terms of the EMT z; however, the experimental Hall-mobility data are not accurate enough to warrant such an analysis. In the lower concentration range $C < 0.4$ the experimental data exhibit a marked deviation from the EMT curve. This is not surprising as the EMT for σ reveals deviations in that range. In the absence of a numerical simulation scheme for R and μ, we have compromised by taking for μ the product of R obtained from EMT and σ as derived from the numerical simulation. The resulting curve, labeled as SBEMT in Fig. 15 substantially improves the agreement with experiment. This is not surprising, as the numerically simulated σ comes quite close to the experimental

values. The deviation of μ (SBEMT) from the ex-
perimental data originates from the (relatively
small) deviation of the experimental R data from
EMT (Fig. 14). This last procedure should not be
taken too seriously; such hybridized theories can
be worse than the EMT, as is the case for the Hall
effect, when one substitutes the simulated value of
f into the EMT formula.

C. Thermal-transport coefficients

We now turn to the analysis of the thermal con-
ductivity[22] and the thermoelectric power[23] for Li
and Na solutions. The available thermal-con-
ductivity data for Na–NH$_3$ can be fitted by the EMT
equation (3.41) with $\kappa_1/\kappa_0 = 0.35$–0.40. The avail-
able experimental data,[22] Fig. 16, are too sparse
and inaccurate to attempt a quantitative correction
for boundary scattering. The negative deviation
of the experimental κ at 7.1 MPM from the EMT
curve indicates that $Z \sim 3$ in Eq. (3.46), a value not
inconsistent with the analysis of the electrical con-
ductivity data in the pseudometallic regime. Final-
ly, it is worthwhile to note that for this system the
high κ_1/κ_0 ratio implies that the EMT for the ther-
mal conductivity is valid throughout the whole C
range.

The thermoelectric power data for Li and Na
solutions, Fig. 17, are in reasonable agreement
with the EMT curve calculated from Eqs. (3.40) and
(3.43) with the parameters $\kappa_1/\kappa_0 = 0.35$, $S_1/S_0 = 20$
for both Li and Na, $\sigma_1/\sigma_0 = 1.2 \times 10^{-3}$ for Li, and
$\sigma_1/\sigma_0 = 2.4 \times 10^{-3}$ for Na. We note in passing that
as the general EMT expression, Eqs. (3.43) and
(3.42) for S involves the local conductivity σ_i,
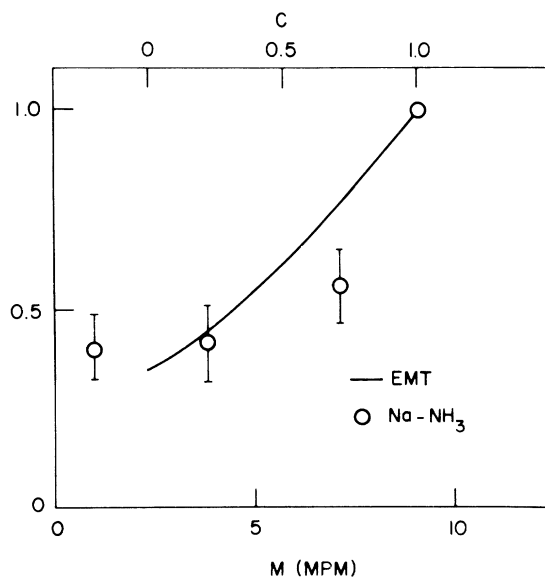which exhibits a large fluctuation for this system,

FIG. 16. Analysis of the available thermal-conductivity
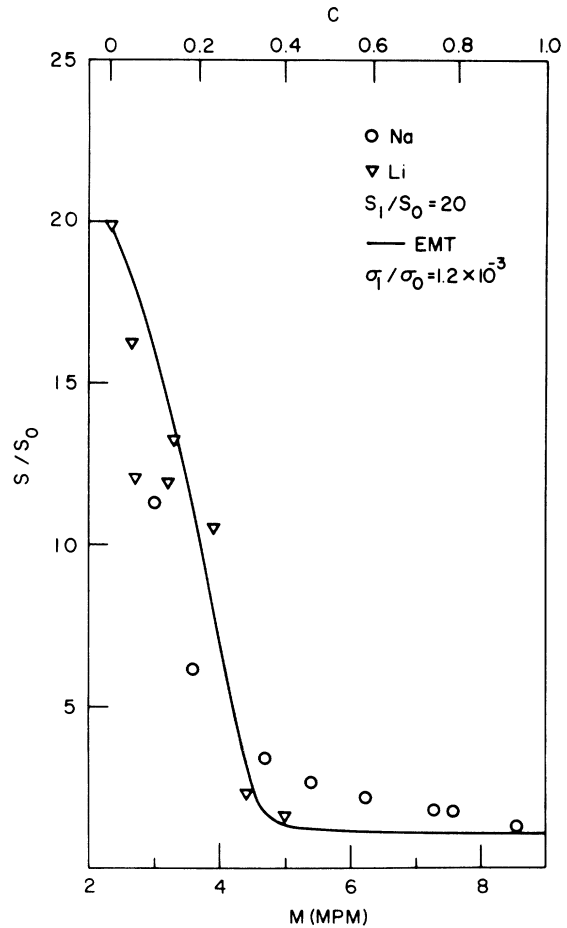data (Ref. 22) for Na–NH$_3$ solutions in terms of the EMT.

FIG. 17. Analysis of the thermoelectric power data
(Ref. 23) for Na–NH$_3$ and for Li–NH$_3$ solutions. The
solid EMT curve is drawn for $S_1/S_0 = 20$, $\kappa_1/\kappa_0 = 0.35$, and
$\sigma_1/\sigma_0 = 1.2 \times 10^{-3}$. Increasing x by a factor of 2 has a
small ($\sim 1\%$) effect in the range $C < 0.4$ where the EMT
is inaccurate.

we do not expect the EMT for S to be as accurate
as for κ for $C < 0.4$.

VII. DISCUSSION

The inhomogeneous state we have proposed to
exist between 2.3 and 9 MPM in Li and Na solutions
at 13 and 8.5 °C above the respective consolute
points has certain remarkable characteristics.
The local concentration has a bimodal distribu-
tion, fluctuating somewhat about two well separated
most probable values, 2.3 and 9 MPM. The pro-
portion of each type of region changes linearly with
average concentration between 2.3 and 9 MPM.
The radius for which the local concentration re-
mains constant before fluctuating randomly to an-
other value is 20 Å from neutron evidence[57] for
Li–ND$_3$ at $T - T_c = 13\,°$C, and 15 Å for Li–NH$_3$ at
$T - T_c = 13\,°$C, and 32 Å for Na–NH$_3$ at $T - T_c$

= 8. 5 °C from interpretation of the data for σ by use of EMT z. None of these values is secure, but they clearly indicate a fluctuation diameter of at least 30 Å for Li–NH$_3$, corresponding to a cluster containing at least 30 ion pairs. The fit to the conductivity data would be far worse than it turned out to be if the two most probable values of local M shifted with mean M or if the distribution of local M values differed significantly from a sharp bimodal distribution. The proposed state therefore resembles a macroscopic mixed phase at a concentration inside a coexistence curve but with the mixing on a microscopic scale. To our knowledge this is the first time such a state of matter has been proposed, and, while all the support for the details of our proposal is indirect, the weight of the evidence seems convincing.

It should be clear that the proposed state has nothing to do with critical fluctuations. Nevertheless, the inhomogeneous state seems to be closely associated with the occurrence of a phase separation. Evidence for inhomogeneity weakens at temperatures further above the consolute point, although there is little data available for quantitative analysis. More to the point, Cs–NH$_3$, which does not have a phase separation,[10] does not appear to exhibit evidence of inhomogeneity,[48] Figs. 4–6.

Three questions are raised implicitly by the above analysis. First, what is the physical origin of the inhomogeneous state? If there is indeed a close association between the inhomogeneous state and the phase separation it is unlikely that the first question can be answered before the second: what is the physical origin of the phase separation? Finally, for Cs or for the other alkali metals at temperatures above those at which the inhomogeneities are important, what is the nature of the metal-nonmetal transition?

With regard to the first two questions, we have demonstrated and will report separately that the complexes present at lower concentrations have substantially dissociated by 2.3 MPM. This leads to dominance of the free energy by a Madelung-like Coulomb contribution, which gives rise to instability at low enough temperatures, providing the driving force for the phase separation. The details of the interplay between the Coulomb interaction and the short-range interactions allow for a shift of the position of maximum instability away from $k = 0$ and provide a possible avenue of explanation of the inhomogeneities.

With regard to the third question, we propose that the metal-nonmetal transition is a Mott transition[38,39,79,80] in the absence of the inhomogeneities we have proposed for Li and Na near and above the region of phase separation. It should be noted, however, that as the Mott transition is taking place in a disordered material,[4] there must be a region
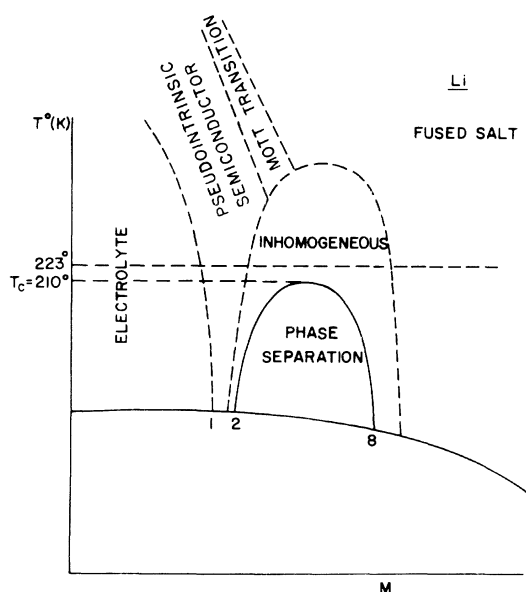

FIG. 18. Sketch of the proposed phase diagram for Li–NH$_3$ solutions.

of the phase diagram over which it is smeared out by inhomogeneities associated with normal, unimodally distributed fluctuations.

We have put all of our proposals together in the form of a phase diagram, Fig. 18. Substantiation of the proposals will require considerable further analysis.

Despite the fact that the MAS are the best studied among systems of comparable level of complexity, there are glaring gaps in our knowledge. We now call attention to those which are most important for confirmation and filling out of our ideas. We have grouped Li and Na together as having an inhomogeneous phase, while Cs does not. We do not know whether Rb even has a phase separation. Chemical potential and small-angle x-ray and neutron scattering studies should be completed in detail for all of the alkali metals. At that point we shall be able to complete the grouping of the remaining alkali metals K and Rb relative to Li and Na and to Cs. K will probably be grouped with Li and Na. We shall need detailed paramagnetic susceptibility data to establish C scales for all of the alkali metals showing inhomogeneities. Similarly, conductivity and Hall-effect data are essential, particularly for Cs to establish differences from Li and Na. Finally, a comparison of optical data for Cs with that available[81] for Na will be of interest.[82]

ACKNOWLEDGMENTS

*Address during August 1–December 31 1974: Chemical Laboratory IV, H. C. Ørsted Institute,

[1] *Metal Ammonia Solutions*, edited by G. Lepoutre and M. J. Siehko (Benjamin, New York, 1964).

[2] *Metal Ammonia Solutions*, edited by J. J. Lagowski and M. J. Sienko (Butterworth, London, 1970).

[3] *Proceedings of Colloque Weyl III on Metal-Ammonia Solutions*, edited by J. Jortner and N. R. Kestner (Springer-Verlag, Heidelberg, 1973), p. 257.

[4] M. H. Cohen and J. C. Thompson, Adv. Phys. $\underline{17}$, 857 (1968).

[5] R. Catteral and N. F. Mott, Adv. Phys. $\underline{18}$, 665 (1969).

[6] MPM refers to mole percent metal.

[7] See, for example, D. A. Copeland, N. R. Kestner, and J. Jortner, J. Chem. Phys. $\underline{53}$, 1189 (1970).

[8] M. Gold, W. L. Jolly, and K. S. Pitzer, J. Am. Chem. Soc. $\underline{84}$, 2264 (1962).

[9] J. L. Dye, Ref. 2, p. 1.

[10] (a) J. C. Thompson, Rev. Mod. Phys. $\underline{40}$, 704 (1968); (b) J. C. Thompson, Ref. 3, p. 231.

[11] The volume expansion data (see Refs. 1–4) indicate that the electron cavities persist in concentrated MAS.

[12] (a) C. A. Kraus, J. Am. Chem. Soc. $\underline{43}$, 741 (1921); (b) C. A. Kraus and W. W. Lucasse, *ibid*. $\underline{43}$, 2529 (1921).

[13] (a) G. Lepoutre and J. P. Lelieur, Ref. 2, p. 247; (b) G. Lepoutre, Ref. 3, p. 181.

[14] J. A. Morgan, J. A. Schroeder, and J. C. Thompson, J. Chem. Phys. $\underline{43}$, 4494 (1965).

[15] (a) R. L. Schroeder, J. C. Thompson, and P. L. Oertel, Phys. Rev. $\underline{178}$, 298 (1969); (b) J. Castel, J. P. Lelieur and G. Lepoutre, J. Phys. (Paris) $\underline{32}$, 211 (1971).

[16] D. S. Kyser and J. C. Thompson, J. Chem. Phys. $\underline{42}$, 3910 (1965).

[17] R. D. Nasby and J. C. Thompson, J. Chem. Phys. $\underline{53}$, 109 (1970).

[18] J. A. Vanderhoff and J. C. Thompson, J. Chem. Phys. $\underline{55}$, 105 (1971).

[19] R. D. Nasby and J. C. Thompson, J. Chem. Phys. $\underline{49}$, 969 (1968).

[20] D. E. O'Reilly, J. Chem. Phys. $\underline{41}$, 3729 (1964).

[21] (a) J. P. Lelieur, Ph.D. thesis (Lille, 1972) (unpublished); (b) J. P. Lelieur, Ref. 2, p. 305; (c) J. P. Leleiur and P. Rigny, J. Chem. Phys. $\underline{59}$, 1142 (1973); (d) J. P. Lelieur, *ibid*. $\underline{59}$, 1148 (1973).

[22] P. G. Varlashkin and J. C. Thompson, J. Chem. Phys. $\underline{38}$, 1904 (1963).

[23] (a) J. F. Dewald and G. Lepoutre, J. Am. Chem. Soc. $\underline{76}$, 3369 (1954); $\underline{78}$, 2956 (1956); (b) J. P. Lelieur, P. Damey, and G. Lepoutre, Ref. 2, p. 203.

[24] (a) J. M. Ziman, Adv. Phys. $\underline{6}$, 551 (1961); (b) T. E. Fober, *ibid*. $\underline{15}$, 547 (1966).

[25] N. F. Mott, Philos. Mag. $\underline{24}$, 1 (1971).

[26] J. C. Thompson, Ref. 1, p. 307.

[27] (a) N. W. Aschroft and G. Russakoff, Phys. Rev. A $\underline{1}$, 39 (1970); (b) R. L. Schroeder and J. C. Thompson, Phys. Rev. $\underline{179}$, 124 (1969).

[28] J. M. Ziman, Philos. Mag. $\underline{6}$, 1013 (1961).

[29] N. F. Mott, Adv. Phys. $\underline{16}$, 49 (1967).

[30] M. H. Cohen, J. Non-Cryst. Solids $\underline{4}$, 391 (1970-.

[31] L. Friedman, J. Non-Cryst. Solids $\underline{6}$, 329 (1971).

[32] U. Even and J. Jortner, Phys. Rev. B $\underline{3}$, 2536 (1973).

[33] M. H. Cohen and J. Jortner, Phys. Rev. Lett. $\underline{30}$, 699 (1973).

[34] M. H. Cohen and J. Jortner, Phys. Rev. A $\underline{10}$, 978 (1974).

[35] (a) M. H. Cohen and J. Jortner, *Proceedings of the Fifth International Conference on Amorphous and Liquid Semiconductors, Garmish*, 1973, edited by J. Stuke and W. Brenig (Taylor and Francis, London, 1973), p. 167; (b) M. H. Cohen and J. Jortner, J. J. Phys. (Paris) $\underline{35}$, C4-345 (1974); (c) J. Jortner and M. H. Cohen, J. Chem. Phys. $\underline{58}$, 5170 (1973).

[36] J. V. Acrivos and N. F. Mott, Philos. Mag. $\underline{24}$, 19 (1971).

[37] J. V. Acrivos, Philos. Mag. $\underline{25}$, 757 (1972).

[38] N. F. Mott, Philos. Mag. $\underline{6}$, 287 (1961).

[39] J. A. Krumhansl, in *Physics of Solids at High Pressures*, edited by C. T. Tomizuka and R. M. Emrich (Academic, New York, 1965), p. 425.

[40] (a) P. Chieux and M. J. Sienko, Ref. 2; (b) P. Chieux and M. J. Sienko, J. Chem. Phys. $\underline{55}$, 566 (1970).

[41] N. F. Mott, Philos. Mag. $\underline{19}$, 835 (1969).

[42] N. F. Mott, Philos. Mag. $\underline{22}$, 7 (1970).

[43] N. F. Mott, Philos. Mag. $\underline{17}$, 1259 (1968).

[44] M. H. Cohen, H. Fritzsche, and S. R. Ovshinsky, Phys. Rev. Lett. $\underline{22}$, 1065 (1969).

[45] J. P. Lelieur, G. Lepoutre, and J. C. Thompson, Philos. Mag. $\underline{26}$, 1205 (1972).

[46] (a) J. P. Lelieur, J. Chem. Phys. $\underline{59}$, 3510 (1973); (b) J. C. Thompson and J. P. Leleiur, J. Phys. (Paris) $\underline{35}$, C4-371 (1974).

[47] S. Kirkpatrick, *Proceedings of the Second International Conference on Liquid Metals, Tokyo*, edited by S. Takeuchi (Taylor and Francis, London, 1972), p. 351. Kirkpatricks interesting proposals for the C scale, $C \propto M$; for the conductivity, $\sigma \propto (C - C^*)^{1.6}$, throughout the entire inhomogeneous regime; and for the Hall coefficient $R \propto P(C)$, where $P(C)$ is the percolation probability, have to be regarded as rough approximations. The essential physical point of a metal–nonmetal transition intermediated by inhomogeneities is contained in his work.

[48] K. Ichikawa and J. C. Thompson, J. Chem. Phys. $\underline{59}$, 1680 (1973).

[49] R. Turner, J. Phys. F $\underline{3}$, L57 (1973).

[50] (a) L. S. Orstein and F. Zernike, Proc. Akad. Sci. (Amsterdam) $\underline{17}$, 793 (1914); (b) L. Landau and E. M. Lifschitz, *Statistical Physics* (Pergamon, New York, 1958).

[51] P. Debye, J. Chem. Phys. $\underline{31}$, 680 (1959).

[52] J. M. Ziman, J. Phys. C $\underline{1}$, 1532 (1968).

[53] (a) S. Kirkpatrick, Phys. Rev. Lett. $\underline{27}$, 1722 (1971); (b) S. Kirkpatrick, Rev. Mod. Phys. $\underline{45}$, 574 (1973).

[54] R. Zallen and H. Scher, Phys. Rev. B $\underline{4}$, 4471 (1971).

[55] V. K. S. Shante and S. Kirkpatrick, Adv. Phys. $\underline{20}$, 325 (1971).

[56] P. W. Schmidt, J. Chem. Phys. $\underline{27}$, 23 (1957).

[57]P. Chieux, Phys. Lett. A **48**, 493 (1974).

[58]M. H. Cohen, in *Proceedings of the Tenth International Conference on Physics of Semiconductors, Cambridge,* 1970, edited by S. K. Keller, J. C. Hensel, and F. Stern (USAEC, Springfield, 1970), p. 645.

[59]T. P. Eggarter and M. H. Cohen, Phys. Rev. Lett. **25**, 807 (1970); **27**, 129 (1971).

[60]T. P. Eggarter, Phys. Rev. A **5**, 2996 (1972).

[61]E. N. Economou, S. Kirkpatrick, M. H. Cohen, and T. P. Eggarter, Phys. Rev. Lett. **25**, 520 (1970).

[62]M. H. Cohen and J. Sak, J. Non-Cryst. Solids **8-10**, 696 (1972).

[63]M. H. Cohen, Ref. 3, p. 257.

[64]H. Weyl, Math Ann. **71**, 441 (1912).

[65]A. S. Skall, B. I. Shklovskii, Zh. Eksp. Teor. Fiz. Pis'ma Red. **17**, 522 (1975) [Sov. Phys.-JETP Lett. **17**, 377 (1973)].

[66]D. A. G. Bruggeman, Ann. Phys. (Leipz.) **24**, 636 (1935).

[67]V. I. Odelevskii, J. Tech. Phys. (USSR) **21**, 678 (1951).

[68]R. Landauer, J. Appl. Phys. **23**, 779 (1952).

[69]H. J. Juretschki, R. Landauer, and J. A. Swanson, J. Appl. Phys. **27**, 838 (1956).

[70]M. H. Cohen and J. Jortner, Phys. Rev. Lett. **30**, 696 (1973).

[71]I. Webman, J. Jortner and M. H. Cohen (unpublished).

[72]M. Hori and F. Yonezawa, J. Math. Phys. **16**, 352, 365 (1975).

[73]C. V. Airapetiants, J. Tech. Phys. **27**, 467 (1957) [Sov. Phys.-Tech. Phys. **2**, 429 (1958)].

[74]M. H. Cohen and J. Jortner (unpublished).

[75]See, for example, J. Ziman, *Electrons and Phonons* (Oxford U.P., New York, 1973).

[76](a) N. F. Mott, Phys. Rev. Lett. **31**, 466 (1973); (b) N. F. Mott, Philos. Mag. **29**, 613 (1974).

[77]Equation (5.2) is an approximation to the correct form

$$M = 9(N_T^0/\bar{N}_{\bar{T}})C + M_1(N_T^1/\bar{N}_{\bar{T}})(1 - C). \qquad (5.2')$$

It is shown below that the best value of M_1 is 2.3 MPM.

For that value, the ratios of the total number densities $\bar{N}_{\bar{T}}$, the average value, and N_T^0, the value in the metallic regions, or N_T^1, the value in the nonmetallic regions, changes only by 6% as M varies from 2.3 to 9 MPM. Inasmuch as the Fig. 9 and 2.3 MPM are no more accurate than that, we chose to ignore the density ratios in (5.2') and used (5.2) instead.

[78]Equation (5.11) can be made more explicit by ignoring exchange enhancement of the susceptibility. K_m is then given by

$$K_m = (\chi_m/N_m)\tfrac{8}{3}\pi \langle | \psi(0) |^2_F \rangle,$$

where $\langle | \psi(0) |^2_F \rangle$ is the probability density for a conduction electron at the nucleus averaged over the Fermi surface within the metallic region. The volume susceptibility χ_m has the Pauli form,

$$\chi_m = \mu_B^2 n_0(E_F),$$

where μ_B is the Bohr magneton. Inserting the two above equations into (5.11) and using (3.5) results in

$$\bar{N}K = \mu_B^2 n(F_F) \langle | \psi(0) |^2_F \rangle + K_1 N_1(1 - C). \qquad (5.11')$$

Thus the metallic contribution to the Knight shift is determined by the average $n(F_F)$ rather than the local $n_0(F_F)$ density of states.

[79]J. Hubbard, Proc. R. Soc. A **276**, 238 (1961); A **281**, 401 (1964).

[80](a) W. Kohn, Phys. Rev. A **133**, 171 (1964); (b) W. Kohn, Phys. Rev. Lett. **19**, 789 (1967); **19**, 439 (1967).

[81]T. A. Beckman and K. S. Pitzer, J. Phys. Chem. **65**, 1527 (1961).

[82]Our physical model provides a clear out explanation for the persistence of the optical absorption band of the solvated electron up to $M = 5.3$ MPM in Na-NH$_3$ solutions (Ref. 81). In this inhomogeneous system the non-metalic-and the metalliclike optical absorption coexist up to $C = 0.5$.